Computers & Structures, Vol. 4, pp. 399–435. Pergamon Press 1974. Printed in Great Britain

STRESS, STABILITY AND VIBRATION OF COMPLEX, BRANCHED SHELLS OF REVOLUTION

DAVID BUSHNELL

Lockheed Palo Alto Research Laboratory, Palo Alto, California, U.S.A.

Abstract—A comprehensive computer program, designated BOSOR4, for analysis of the stress, stability and vibration of segmented, ring-stiffened, branched shells of revolution and prismatic shells and panels is described. The program performs large-deflection axisymmetric stress analysis, small-deflection nonsymmetric stress analysis, modal vibration analysis with axisymmetric nonlinear prestress included, and buckling analysis with axisymmetric or nonsymmetric prestress. One of the main advantages of the code is the provision for realistic engineering details such as eccentric load paths, internal supports, arbitrary branching conditions, and a 'library' of wall constructions. The program is based on the finite-difference energy method which is very rapidly convergent with increasing numbers of mesh points. The organization of the program is briefly described with flow of calculations charted for each of the types of analysis. Overlay charts and core storage requirements are given for the CDC 6600, IBM 370/165, and UNIVAC 1108 versions of BOSOR4. A large number of cases is included to demonstrate the scope and practicality of the program period.

INTRODUCTION

THE PURPOSE of this paper is to describe a computerized method of analysis for composite, branched shells of revolution. The main advantage of the analysis method and computer program is its direct and efficient applicability to practical engineering design problems involving very complex shells of revolution or prismatic shell structures such as corrugated panels or noncircular cylinders. Emphasis is placed on analytical results for a variety of 'real-world' engineering problems. Details of the analysis method are reported in Ref. [1].

Extensive literature exists on analysis and computer programs for shells and solids of revolution. Figure 1 contains the names of many computer programs and names of originators of other computer programs that cover this field. The names are given in a 'coordinate system' arranged such that increasingly 'general purpose' computer codes lie increasing distances from both axes. Other codes, existing just outside of the region depicted, apply to structures that are 'almost' shells of revolution, such as shells with cutouts, shells with material properties that vary around the circumference, or panels of shells of revolution.

The region shown in Fig. 1 is divided by a heavy line into two fields: Programs lying within the heavy line are based on numerical methods that are essentially one-dimensional, that is, the dependent variables are separable and only one spatial variable need be discretized; programs lying outside the heavy line are based on numerical methods in which two spatial variables are discretized. It is generally true that analysis methods and programs lying outside the heavy line require perhaps an order of magnitude more computer time for a given case with given nodal point density than do those lying inside the line. This distinction arises because the bandwidths and ranks of equation systems in two-dimensional numerical analyses are greater than those in one-dimensional numerical analyses. Certain of the areas in Fig. 1 are blank. Those near the origin correspond in general to cases for

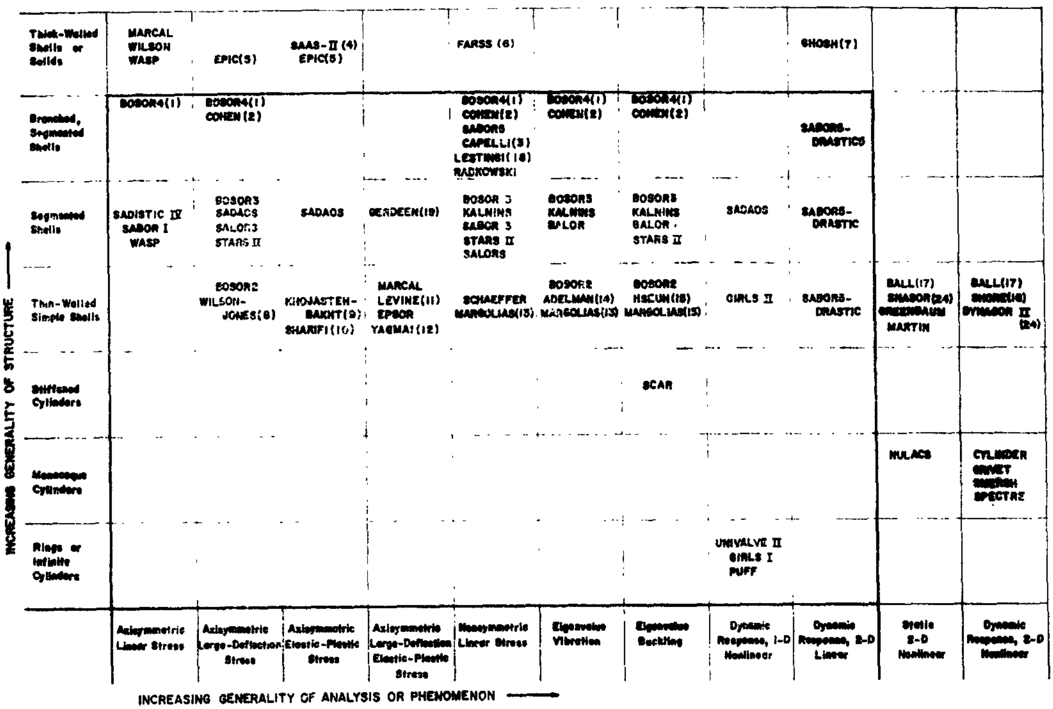

FIG. 1. Computer programs for shells and solids in revolution.

which closed-form solutions exist and for which slightly more general programs are clearly applicable. The blank areas lying near the outer boundaries of the chart are for the most part covered by more general programs such as NASTRAN, SNAP, REXBAT, STAGS, STRUDL, and ASKA [20].

The numerals next to the program name or to the originator names correspond to references at the end of the text. Names shown with no numerals are referenced in one or more of the survey papers, Refs. [20–23]. These papers describe the various numerical procedures used, and in one case [21] hint as to the availability of some of the codes.

This paper will focus on a description of the general branched shell-of-revolution analyzer called BOSOR4. The goals of the research leading to the BOSOR4 code have been to provide as general as possible an engineering tool within the restriction of one-dimensional discretization; to include as much capability as possible for analysis of practical engineering structures, which include meridional discontinuities, weld mismatches, composite materials, discrete rings, sliding constraints, etc. to make the computer program easy to use by means of logical arrangement of input data, internal diagnostics, plots, and a complete user's manual; to make the code as efficient as possible; and to maximize its availability by converting it and checking it out on three major systems—the Univac 1108, the CDC 6600, and the IBM 370/165. Program tapes and manuals are available through the author or through the COSMIC system. Described in this paper are the scope of BOSOR4, the analysis method, and the program organization; in addition, several cases involving nonlinear stress analysis, buckling, and vibration of segmented, branched, ring-stiffened shells of revolution with various wall constructions are discussed.

SCOPE OF THE BOSOR4 COMPUTER PROGRAM

The BOSOR4 code performs stress, stability, and vibration analyses of segmented, branched, ring-stiffened, elastic shells of revolution with various wall constructions. Figure 2 shows some examples of branched structures which can be handled by BOSOR4. Figure 2a represents part of a multiple-stage rocket treated as a shell of seven segments; Fig. 2b represents part of a ring-stiffened cylinder in which the ring is treated as two shell segments branching from the cylinder; Fig. 2c shows the same ring-stiffened cylinder, but with the ring treated as 'discrete', that is the ring cross section can rotate and translate but not deform, as it can in the model shown in Fig. 2b. Figures 2d–f represent branched prismatic shell structures, which can be treated as shells of revolution with very large mean circumferential radii of curvature, as described in Ref. [25] and later in this paper.

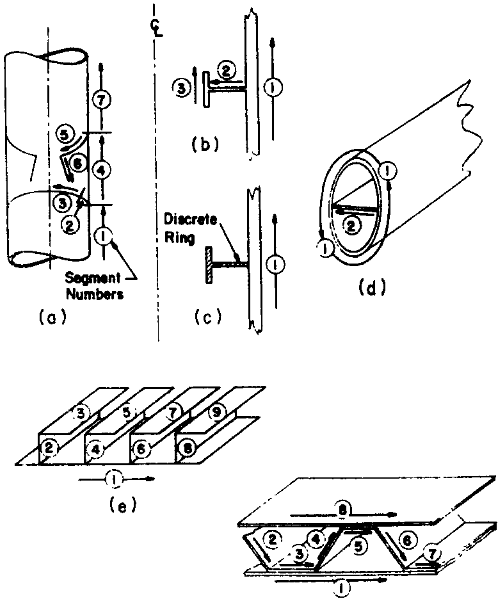

FIG. 2. Examples of branched structures which can be analyzed with BOSOR4.

The program is very general with respect to geometry of meridian, shell-wall design, edge conditions, and loading. It has been thoroughly checked out by comparisons with other known solutions and tests. The BOSOR4 capability is summarized in Table 1. The code represents three distinct analyses:

(1) A nonlinear stress analysis for axisymmetric behavior of axisymmetric shell systems (large deflections, elastic)

(2) A linear stress analysis for axisymmetric and nonsymmetric behavior of axisymmetric shell systems submitted to axisymmetric and nonsymmetric loads

(3) An eigenvalue analysis in which the eigenvalues represent buckling loads or vibration frequencies of axisymmetric shell systems submitted to axisymmetric loads. (Eigenvectors may correspond to axisymmetric or nonsymmetric modes.)

TABLE 1. BOSOR4 capability summary

Type of analysis	Shell geometry	Wall construction	Loading
Nonlinear axisymmetric stress Linear symmetric or nonsymmetric stress Stability with linear symmetric or nonsymmetric prestress or with nonlinear symmetric prestress Vibration with nonlinear prestress analysis Variable mesh point spacing within each segment	Multiple-segment shells, each segment with its own wall construction, geometry, and loading Cylinder, cone, spherical, ogival, toroidal, ellipsoidal, etc. General meridional shape; point-by-point input Axial and radial discontinuities in shell meridian Arbitrary choice of reference surface General edge conditions Branched shells Prismatic shells and composite built-up panels	Monocoque, variable or constant thickness Skew-stiffened shells Fiber-wound shells Layered orthotropic shells Corrugated, with or without skin Layered orthotropic with temperature-dependent material properties Any of above wall types reinforced by stringers and/or rings treated as "smeared out" Any of above wall types further reinforced by rings treated as discrete Wall properties variable along meridian	Axisymmetric or nonsymmetric thermal and/or mechanical line loads and moments Axisymmetric or nonsymmetric thermal and/or mechanical distributed loads Proportional loading Non-proportional loading

BOSOR4 has an additional branch corresponding to buckling of nonsymmetrically loaded shells of revolution. However, this branch is really a combination of the second and third analyses just listed.

In the BOSOR4 code, the user chooses the type of analysis to be performed by means of a control integer INDIC:

INDIC$=-2$ Stability determinant calculated for given circumferential wave number N for increasing loads until it changes sign. Nonlinear prebuckling effects included. INDIC then changed automatically to -1 and calculations proceed as if INDIC has always been -1.

INDIC$=-1$ Buckling load and corresponding wave number N determined, including nonlinear prebuckling effects. N corresponding to *local* minimum critical load $L_{cr}(N)$ is automatically sought.

INDIC$=0$ Axisymmetric stresses and displacements calculated for a sequence of stepwise increasing loads from some starting value to some maximum value, including nonlinear effects. Axisymmetric collapse loads can be calculated.

INDIC$=1$ Buckling loads calculated with nonlinear bending theory for a *fixed* load. Buckling loads calculated for a range of circumferential wave numbers. Several buckling loads for each wave number can be calculated.

INDIC=2 Vibration frequencies and mode shapes calculated, including the effects of prestress obtained from axisymmetric nonlinear analysis. Several frequencies and modes can be calculated for each circumferential wave number.

INDIC=3 Nonsymmetric or symmetric stresses and displacements calculated for a range of circumferential wave numbers. Linear theory used. Results for each harmonic are automatically superposed. Fourier series for nonsymmetric loads are automatically computed or may be provided by user.

INDIC=4 Buckling loads calculated for nonsymmetrically loaded shells. Prebuckled state obtained from linear theory (INDIC=3) or read in from cards. 'Worst' meridional prestress distribution (such as distribution involving maximum negative meridional or hoop prestress resultant) chosen by user, and this particular distribution is assumed to be axisymmetric in the stability analysis, which is the same as that for the branch INDIC=1.

The variety of buckling analyses (INDIC=−2, −1, 1, and 4) is provided to permit the user to approach a given problem in a number of different ways. There are cases for which an INDIC=−1 analysis, for example, will not work. The user can then resort to an INDIC=−2 analysis, which requires more computer time, but which is generally more reliable. Buckling of a shallow spherical cap under external pressure is an example. In an INDIC=−1 analysis of the cap, the program generates a sequence of loads that ordinarily should converge to the lowest buckling load, with nonlinear prebuckling effects included. Depending on the cap geometry and the user-provided initial pressure, however, one of the loads in the sequence may exceed the axisymmetric collapse pressure of the cap. This phenomenon can occur if the bifurcation buckling loads are just slightly smaller than the axisymmetric collapse loads. The user can obtain a solution with use of INDIC=−2, in which the bifurcation load is approached from below in a 'gradual' manner. The BOSOR4 manual [1] contains an example of this case. A somewhat different illustration is provided in the section on analytical results.

The branch INDIC=1 is provided because it is sometimes desirable to know several buckling eigenvalues for each circumferential wave number, N, and because there may exist more than one minimum in the critical load vs N-space. This is especially true for composite shell structures with many segments and load types. Such a structure can buckle in many different ways. The designer may have to eliminate several possible failure modes, not just the one corresponding to the lowest pressure, for example. The INDIC=4 branch is provided for two reasons: The user can calculate buckling under nonsymmetric loads without having to make two separate runs, an INDIC=3 run and an INDIC=1 run. In addition, this branch permits the user to bypass the prebuckling analysis and read prebuckling stress distributions and rotations directly from cards. This second feature is very useful for the treatment of composite branched panels under uniaxial or biaxial compression.

The BOSOR4 program, although applicable to shells of revolution, can be used for the buckling analysis of composite, branched panels by means of a 'trick' described in detail in Ref. [25]. This 'trick' permits the analysis of any prismatic shell structure that is simply-supported at particular stations along the length. Any boundary conditions can be used along generators. In Ref. [25] many examples are given, including nonuniformly loaded cylinders,. noncircular cylinders, corrugated panels, and cylinders with stringers treated as discrete. This paper gives other examples.

ANALYSIS METHOD

The assumptions upon which the BOSOR4 code is based are:

(1) The wall material is elastic.
(2) Thin-shell theory holds; i.e. normals to the undeformed surface remain normal and undeformed.
(3) The structure is axisymmetric, and in vibration analysis and nonlinear stress analysis the loads and prebuckling or prestress deformations are axisymmetric.
(4) The axisymmetric prebuckling deflections in the nonlinear theory (INDIC=0, −1, 2), while considered finite, are moderate; i.e. the square of the meridional rotation can be neglected compared with unity.
(5) In the calculation of displacement and stresses in nonsymmetrically loaded shells (INDIC=3), linear theory is used. This branch of the program is based on standard small-deflection analysis.
(6) A typical cross-section dimension of a discrete ring stiffener is small compared with the radius of the ring.
(7) The cross-sections of the discrete rings remain undeformed as the structure deforms, and the rotation about the ring centroid is equal to the rotation of the shell meridian at the attachment point of the ring (except, of course, if the ring is treated as a flexible shell branch).
(8) The discrete ring centroids coincide with their shear centers.
(9) If meridional stiffeners are present, they are numerous enough to include in the analysis by an averaging or 'smearing' of their properties over any parallel circle of the shell structure, meridional stiffeners can be treated as discrete though the 'trick' described in Ref. [25].

The analysis is based on energy minimization with constraint conditions. The total energy of the system includes strain energy of the shell segments and discrete rings, potential energy of the applied line loads and pressures, and kinetic energy of the shell segments and discrete rings. The constraint conditions arise from displacement conditions at the boundaries of the structure, displacement conditions that may be prescribed anywhere within the structure, and at junctures between segments. The constraint conditions are introduced into the energy functional by means of Lagrange multipliers.

These components of energy and constraint conditions are initially integro–differential forms. The circumferential dependence is eliminated by separation of variables. Displacements and meridional derivatives of displacements are then written in terms of the shell reference surface displacement components u_i, v_i and w_i at the finite-difference mesh points and Lagrange multipliers λ_i. Integration is performed simply by multiplication of the energy per unit length of meridian by the length of the 'finite difference element', to be described below.

In the nonlinear axisymmetric stress analysis the energy expression has terms linear, quadratic, cubic, and quartic in the dependent variables u_i and w_i. The cubic and quartic energy terms arise from the 'rotation-squared' terms that appear in the expression for reference surface meridional strain and in the constraint conditions. Energy minimization leads to a set of nonlinear algebraic equations that are solved by the Newton–Raphson method. Stress and moment resultants are calculated in a straightforward manner from the mesh-point displacement components through the constitutive equations and the kinematic relations.

The results from the nonlinear axisymmetric or linear nonsymmetric stress analysis are used in the eigenvalue analyses for buckling and vibration. The 'prebuckling' or 'prestress' meridional and circumferential stress resultants N_{10} and N_{20} and the meridional rotation χ_0 appear as known variable coefficients in the energy expressions that govern buckling and vibration. These expressions are homogeneous quadratic forms. The values of a parameter (load or frequency) that render the quadratic forms stationary with respect to infinitesimal variations of the dependent variables represent buckling loads or natural frequencies. These eigenvalues are calculated from a set of linear homogeneous equations. More will be written about the bifurcation buckling eigenvalue problems in the following paragraphs.

Details of the analysis are given in Refs. [1, 26 and 27]. Only three aspects will be described here: the 'finite-difference element', the form of the stability eigenvalue problem, and the effect of branched systems on the configuration of the stiffness matrix.

THE 'FINITE-DIFFERENCE' ELEMENT

BOSOR4 is based on the finite-difference energy method. This method is described in detail and compared with the finite element method in Ref. [28]. Figure 3 shows a typical shell segment meridian with finite-difference mesh points. The 'u' and 'v' points are located halfway between adjacent 'w' points. The energy contains up to first derivatives in u and v and up to second derivatives in w. Hence, the shell energy density evaluated at the point labeled E (center of the length l) involves the seven points w_{i-1} through w_{i+1}. The energy per unit circumferential length is simply the energy per unit area multiplied by the length

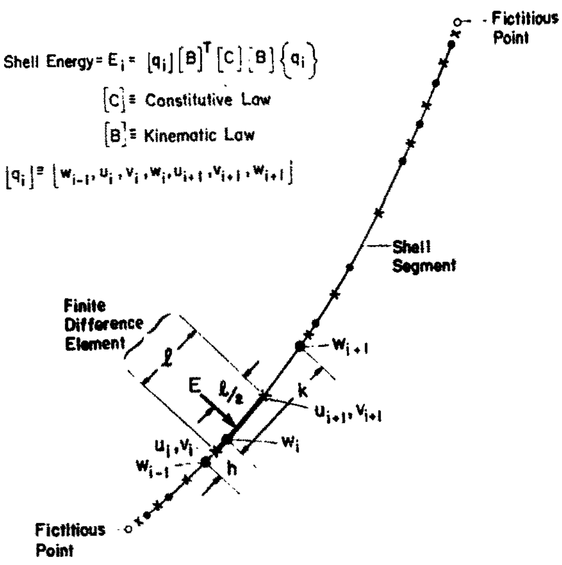

FIG. 3. Finite-difference discretization: the 'finite-difference element'.

of the finite-difference element l, which is the arc length of the reference surface between two adjacent u or v points. In Ref. [28] it is shown that this formulation yields a (7×7) stiffness matrix corresponding to a constant–strain, constant–curvature-change finite element that is incompatible in normal displacement and rotation at its boundaries but that in general gives very rapidly convergent results with increasing density of nodal points. Note that two of the w-points lie outside of the element. If the mesh spacing is constant, the algebraic equations obtained by minimization of the energy with respect to nodal degrees-of-freedom can be shown to be equivalent to the Euler equations of the variational problem in finite form. Further description and proofs are given in Ref. [28].

Figures 4 and 5 show rates of convergence with increasing nodal point density for a

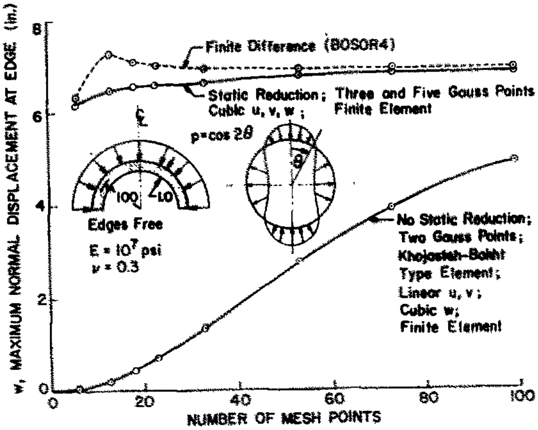

FIG. 4. Normal displacement at free edge of hemisphere with nonuniform pressure $p(s, \theta)=p_0 \cos 2\theta$.

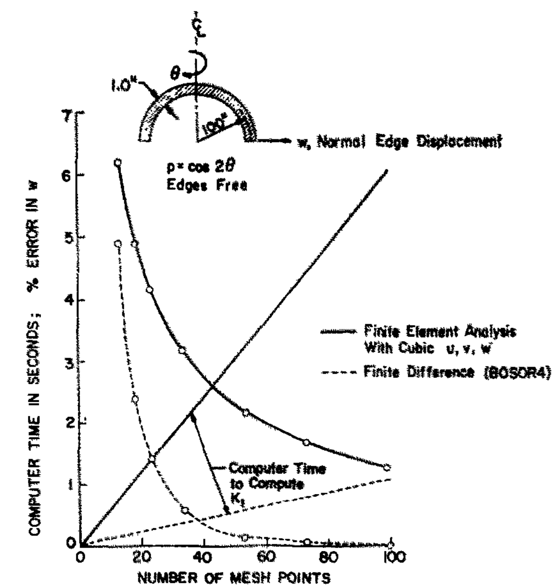

FIG. 5. Computer times to form stiffness matrix K_1 and rates of convergence of normal edge displacement for free hemisphere with nonuniform pressure $p(s, \theta)=p_0 \cos 2\theta$.

poorly conditioned problem—a stress analysis of a thin, nonsymmetrically loaded hemisphere with a free edge. The finite-element results were obtained by programming various kinds of finite elements into BOSOR4. The computer time for computation of the stiffness matrix K_1 is shown in Fig. 5. A much smaller time for computation of the finite-difference K_1 is required because there are fewer calculations for each 'Gaussian' integration point and because there is only one 'Gaussian' point per finite-difference element. Other comparisons of rate of convergence with the two methods used in BOSOR4 are shown for buckling and vibration problems in Ref. [28].

FORMULATION OF THE STABILITY PROBLEM

The bifurcation buckling problem represents perhaps the most difficult of the three types of analyses performed by BOSOR4. It is practical to consider bifurcation buckling of complex, ring-stiffened shell structures under various systems of loads, some of which are considered to be known and constant, or 'fixed' and some of which are considered to be unknown eigenvalue parameters, or 'variable'.

The notion of 'fixed' and 'variable' systems of loads not only permits the analysis of structures submitted to nonproportionally varying loads, but also helps in the formulation of a sequence of simple of 'classical' eigenvalue problems for the solution of problems governed by 'nonclassical' eigenvalue problems. An example is a shallow spherical cap under external pressure. Very shallow caps fail by nonlinear collapse, or snap-through buckling, not by bifurcation buckling. Deep spherical caps fail by bifurcation buckling in which nonlinearities in prebuckling effects are not particularly important. There is a range of cap geometries for which bifurcation buckling is the mode of failure and for which the critical pressures are very much affected by nonlinearities in prebuckling behavior. The analysis of this intermediate class of spherical caps is simplified by the concept of 'fixed' and 'variable' pressure

Figure 6 shows the load-deflection curve of a shallow cap in this intermediate range. Nonlinear axisymmetric collapse (p_{nl}), linear bifurcation (p_{lb}), and nonlinear bifurcation (p_{nb}) loads are shown. The purpose of the analysis referred to in this section is to determine the pressure p_{nb}. It is useful to consider the pressure p_{nb} as composed of two parts

$$p_{nb}=p^f+p^v$$

in which p^f denotes a known or 'fixed' quantity, and p^v denotes an undetermined or 'variable' quantity. The fixed portion p^f is an initial guess or represents the results of a previous iteration. The variable portion p^v is the remainder, which can be determined from a reasonably simple eigenvalue problem, as will be described. It is clear from Fig. 7 that if p^f is fairly close to p_{nb} the behavior in the range $p=p^f \pm p^v$ is reasonably linear. Thus, the eigenvalue p_{nb} can be calculated by means of a sequence of eigenvalue problems through which ever and ever smaller values p^v are determined and added to the known results p^f from the previous iterations. As the BOSOR4 computer program is written the initial guess p^f need not be close to the solution p_{nb}.

In the bifurcation stability analysis it is necessary to develop three matrices corresponding to the eigenvalue problem

$$K_1x+\lambda K_2x+\lambda^2K_3x=0. \tag{1}$$

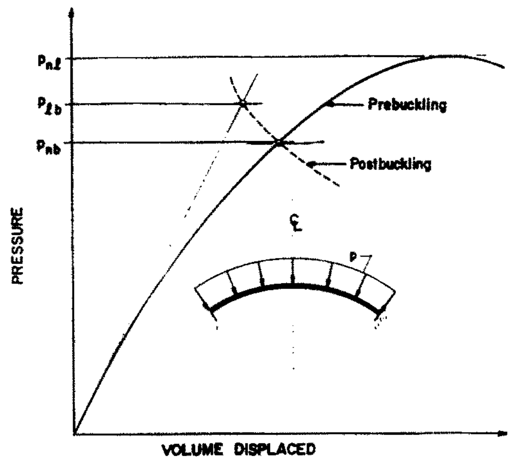

FIG. 6. Load-deflection curves for shallow spherical cap, showing bifurcation points from linear prebuckling curve (p_{lb}) and nonlinear prebuckling curve (p_{nb}).

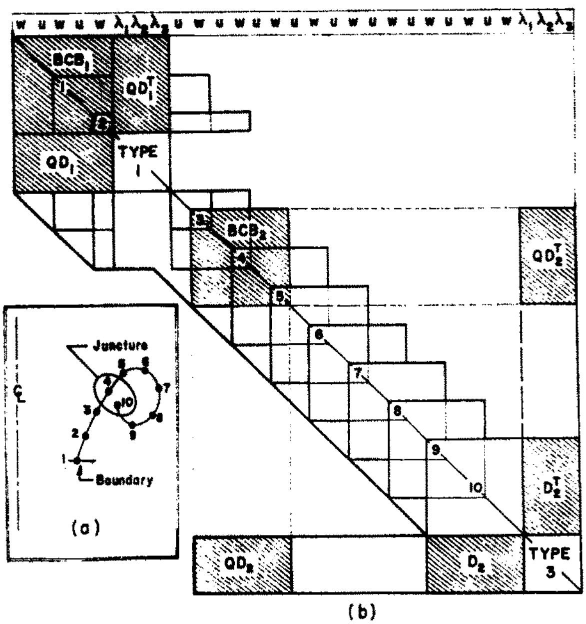

FIG. 7. Stiffness matrix configuration with types 1 and 3 constraint conditions.

The matrix K_1 is the stiffness matrix and contains 'fixed' load effects; the matrix K_2 is commonly called the 'load-geometric' matrix and contains linear terms involving the 'variable' loads; and the matrix K_3, another 'variable'-load quantity, is called the λ^2-matrix, for obvious reasons. These matrices all contain known numbers and are all banded.

The bifurcation buckling problem is stated mathematically in terms of the second variation of the total energy. For a shell the second variation is given by

$$\delta^2 U=\int_s\int_\theta\Bigg[[\varepsilon^1][C]\{\varepsilon^1\}+[\varepsilon^2][C]\{\varepsilon^0\}+[\varepsilon^0][C]\{\varepsilon^2\}+2[N^T]\{\varepsilon^2\} +[\delta u,\ \delta v,\ \delta w][P]\begin{bmatrix}\delta u\\ \delta v\\ \delta w\end{bmatrix}\Bigg]r\mathrm{d}\theta\mathrm{d}s \qquad (2)$$

in which ε^0, ε^1, ε^2 signify, respectively, strain vectors (containing reference surface strains and changes in curvature) that are zeroth, first, and second order in the displacement variations δu, δv, δw and that contain prebuckling quantities; $[C]$ represents the 6×6 matrix of stress–resultant–strain coefficients; N^T represents thermal effects; $[P]$ represents 'pressure–rotation' effects; s and θ are the meridional and circumferential coordinates, respectively; and r is the local parallel circle radius of the shell of revolution.

The linear part of the 'strain increment during buckling', ε^1, contains the prebuckling meridional rotation χ_0. The prebuckling strain vector ε^0 contains terms both linear and quadratic in prebuckling rotations. If, in a reasonably small neighborhood $(\ )^v$ of a known prebuckling state $(\ )^f$, the behavior of the shell can be considered linear with respect to load, then in this neighborhood the second variation of the shell strain energy can be written in the form

$$\delta^2 U=\int_s\int_\theta (A_1+\lambda A_2+\lambda^2 A_3)r\mathrm{d}s\mathrm{d}\theta. \qquad (3)$$

Formulas for A_1, A_2 and A_3 are given in Ref. [1]. The development is expanded in Ref. [1] to include discrete ring strain energy and constraint conditions. If the integration is performed and the second variation is 'minimized' with respect to the dependent variables δu_i, δv_i, δw_i, and the Lagrange multipliers, the eigenvalue problem of equation (1) results. The method of solution of this problem is described in Ref. [1]. An eigenvalue problem of the same form was derived and solved by Anderson *et al.* [29]. Eigenvalues are extracted by means of the method of inverse power iterations with spectral shifts.

STIFFNESS MATRICES FOR BRANCHED SYSTEMS

Figures 7–10 show the configurations of stiffness matrices for various types of branching conditions. These matrices are specifically for prebuckling axisymmetric problems in which only u and w displacement components exist, and for which there are only three equations for each constraint point (u, w, and rotation compatibility). However, the forms of stability or vibration or nonsymmetric stress stiffness matrices are similar, the only differences being that the 'point' stiffness matrices are 7×7 rather than 5×5, and there are four lambda's for each boundary or juncture condition rather than three. In Figs. 7 and 8 the 5×5 element squares 'BCB' represent 'local' stiffness matrices contributed by each finite-difference element (see Fig. 3). The rectangular 3×5 and 5×3 matrices 'QD' and 'D' represent the constraint conditions obtained by minimization of the energy with respect to the Lagrange multipliers. The shaded blocks receive contributions from the constraint conditions. Reference [1] shows what the various contributions are.

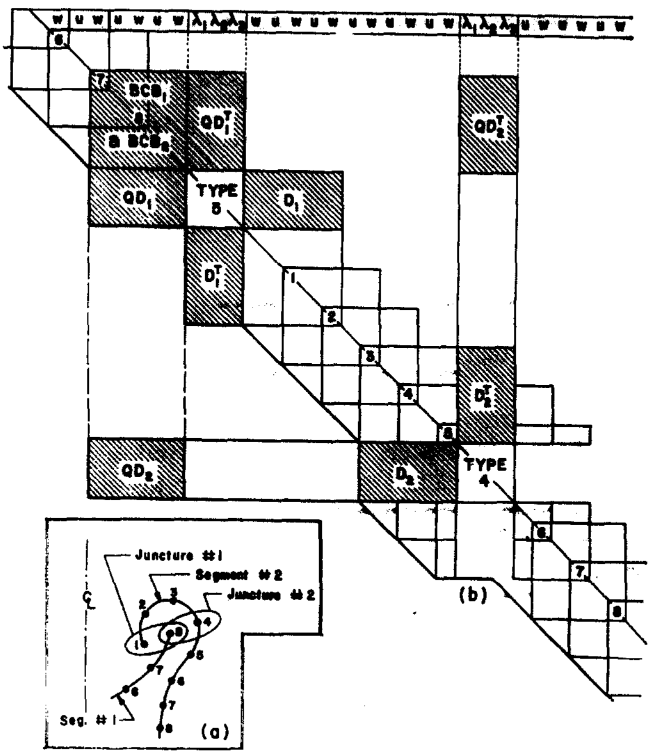

FIG. 8. Stiffness matrix configuration with type 4 and 5 constraint conditions.

There are five types of constraint conditions recognized by BOSOR4: Type 1 is a simple 'one-sided' constraint condition (e.g., boundary condition) not at the termination of a segment (it can be at the beginning as in Fig. 7); Type 2 is a simple 'one-sided' constraint condition (boundary condition) at the termination of a segment (shown in Fig. 10, Seg. 1); Type 3 is a juncture condition in which the termination of a segment is connected in some way to a nonadjacent previous point (Fig. 7); Type 4 is a juncture condition in which a point embedded within a segment is connected to a nonadjacent previous point (Fig. 8); and Type 5 is a juncture condition in which the termination of Segment (i) is connected to the beginning of Segment $(i+1)$. Figure 9a shows a stiffness matrix configuration that would result for a complete toroidal shell held at one point; 9b gives an example of a meridian free at the boundaries and constrained at an interior point. Figure 10 shows a stiffness matrix configuration corresponding, for example, to a corrugated semisandwich panel in which the corrugations are riveted to the flat sheet at intervals along the surface. Other examples are given in Ref. [1].

BOSOR4 PROGRAM ORGANIZATION

The BOSOR4 program consists of a main program MAIN and six overlays called READIT, PRE, ARRAYS, BUCKLE, MODE1, AND PLOT1. Figure 11 shows the Univac 1108/EXEC8 and IBM 370/165 program organization. The program structure for the CDC 6600 is similar, except that READIT contains one (rather than two) tiers of

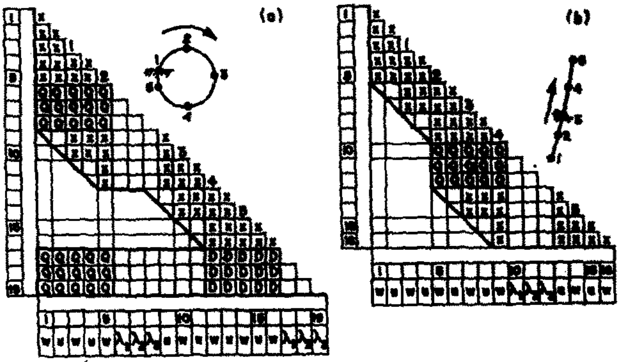

FIG. 9a. Stiffness matrix configuration for shell with closed meridian supported at point 1; (b) for meridian supported at interior point.

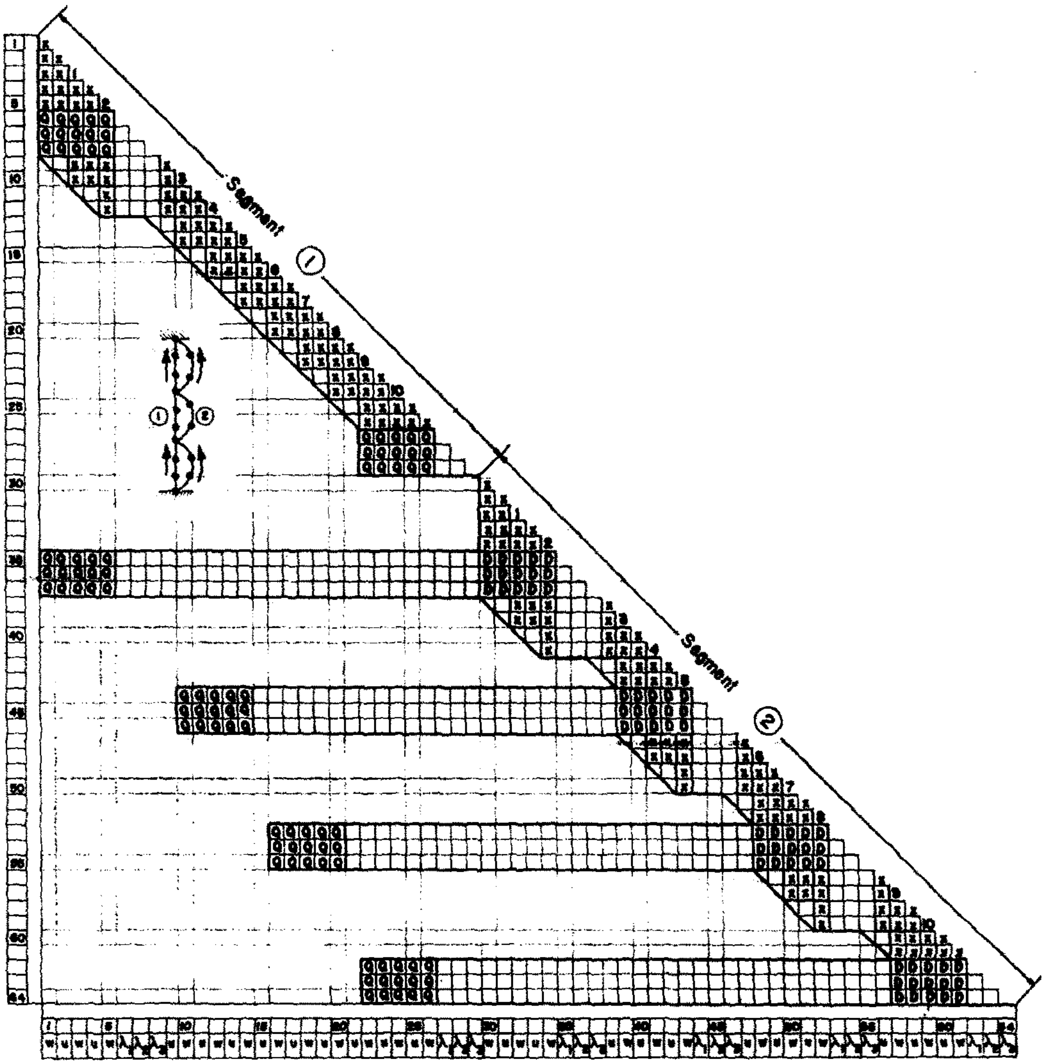

FIG. 10. Stiffness matrix configuration for double-walled shell fastened intermittently.

overlays (Fig. 12). Figure 12 gives the core storage in decimal words required for the Univac 1108, IBM 370, and CDC 6600 versions of BOSOR4. The Univac 1108 and IBM 370 versions are written in double precision FORTRAN IV; the CDC version is written in single precision FORTRAN IV. In Fig. 11, a box around a subroutine name indicates that it calls other subroutines.

Overall control in BOSOR4 depends on the integer INDIC. The various types of analysis chosen by the input variable INDIC are listed in a previous section, and the flow of calculations for each value of INDIC is given in Fig. 13†. All of the input data are read in READIT. Figure 14 shows all of the subroutines called in this overlay, and Fig. 15 shows the arrangement of a sample data deck. A call to READIT also causes results of calculations to be printed out (OUTFIN). Some general data that pertain to the entire shell are read in first. Then, for each shell segment the mesh point distribution (MESH), meridian geometry (GEOMTR), discrete ring properties (RGDATA), mechanical and thermal line loads (LINELD), mechanical and thermal distributed loads (DISTL), and shell wall properties (WALLS) are read in. The subroutine GASP, which is called in several places, causes certain data to be stored on and read from drum or disk. These data will be used in the calculations to be performed in other overlays. The calculations in READIT are performed in single precision. Overlay READIT has another important function—it causes to be computed 'templates' of the stiffness, load-geometric, lambda-squared, and mass matrices for the nonsymmetric stress, buckling, and vibration problems and the

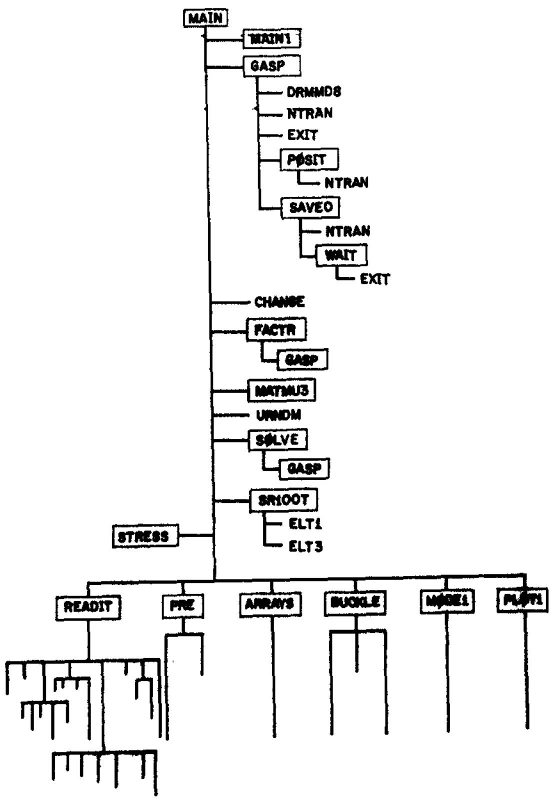

FIG. 11. Main link with overlays.

† Figure 13 appears facing p. 424.

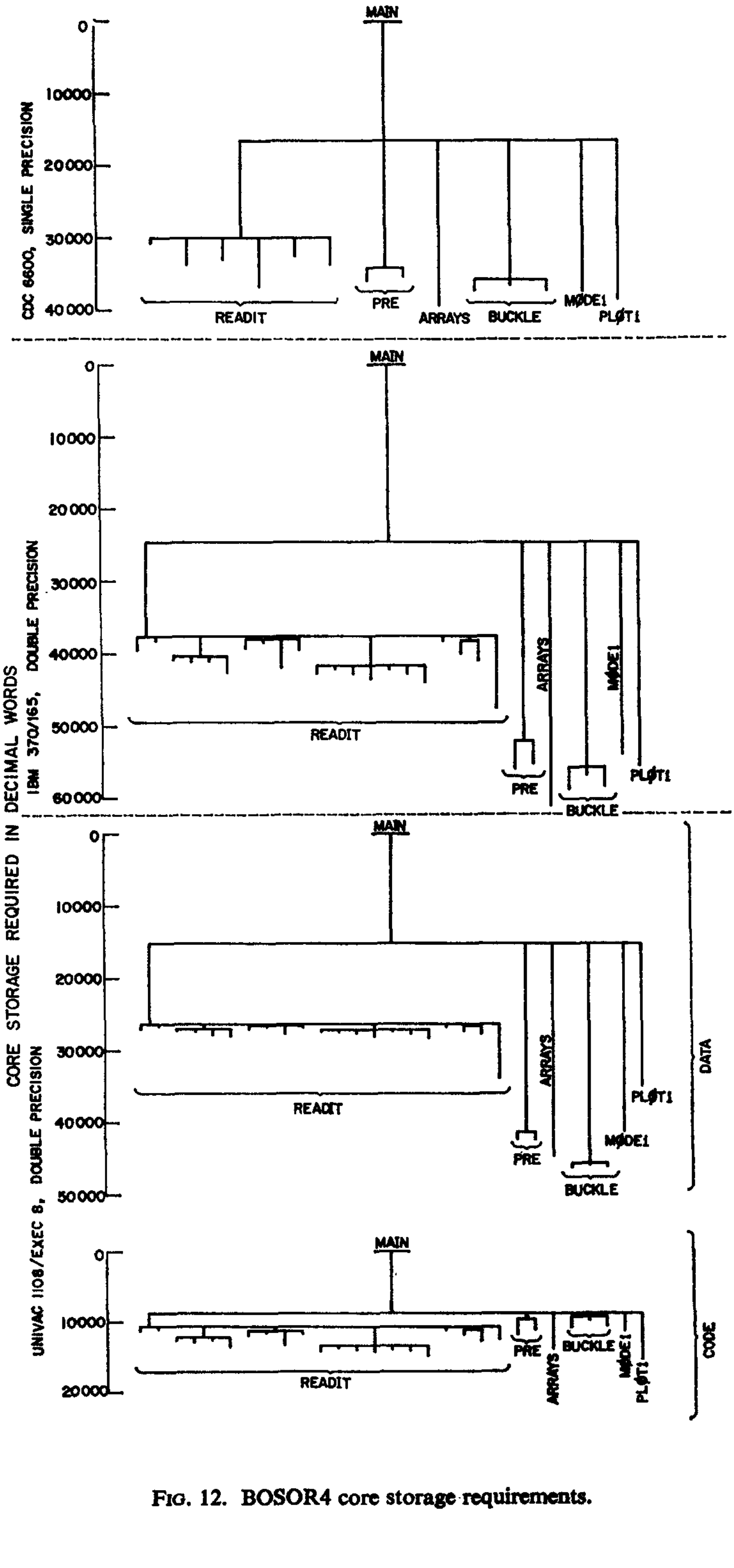

FIG. 12. BOSOR4 core storage requirements.

stiffness matrix for the prebuckling problem. These 'templates' give the 'shapes' of the governing equation systems. Examples are shown in Figs. 7–10.

The nonlinear stress analysis for axisymmetric behavior of axisymmetric systems is performed in the overlay PRE. Data for shell and discrete ring properties, temperature and pressure distributions, and thermal and mechanical line loads are read into core from drum or disk (GASP); 'variable' loads are increased or decreased by appropriate increments or decrements; the coefficient matrix and the 'right-hand-side' vector are derived for the current Newton–Raphson iteration; the coefficient matrix is factored (FACTR); the equation system is solved (SOLVE); a test for convergence is made; and the prebuckling or prestress stress resultants and stresses are calculated from the converged displacement vector. These prestress quantities are stored on the drum or disk for later use in the buckling and vibration analysis and for later plotting.

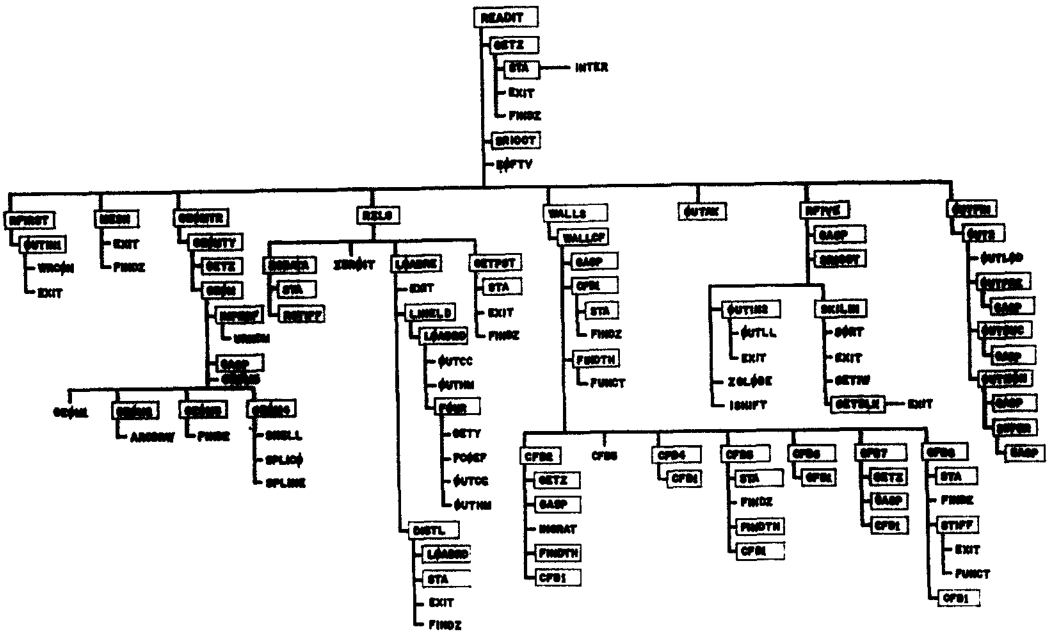

FIG. 14. READIT overlay.

In the next overlay (ARRAYS), the coefficient matrices corresponding to the buckling analysis, vibration analysis, and linear symmetric and nonsymmetric stress analysis are derived. Subroutine ARRAYS is called for each value of the circumferential wave number N. If INDIC=3, the load vector Q, is calculated in ARRAYS, and the linear system $K_1x = Q$ is solved for the given circumferential wave number N. Depending on INDIC, various coefficient matrices are derived. With buckling analyses, for example, three matrices are obtained in ARRAYS for each circumferential wave number N: the stiffness matrix K_1 for the composite shell, which corresponds to the structure loaded by the 'fixed' parts of the loads, the 'load-geometric' matrix K_2 which contains linear powers of the eigenvalue λ, and the 'λ^2' matrix K_3, which contains quadratic powers of λ. In modal vibration analysis, two matrices are derived in ARRAYS: the stiffness matrix K_1 for the prestressed shell, and the mass matrix M. The arrays K_1, K_2, K_3, and M, are stored on drum or disk in blocks of a given length for later use in overlay BUCKLE.

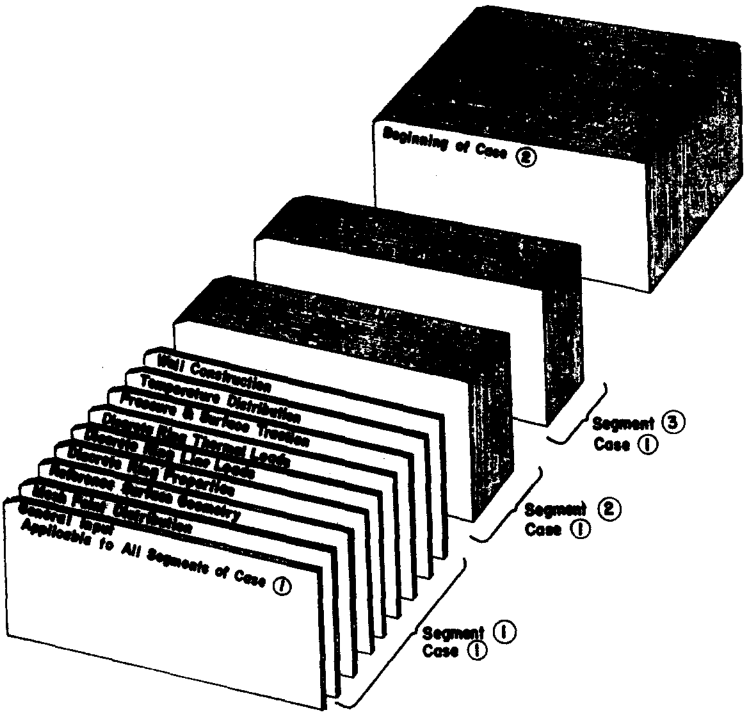

FIG. 15. Sample data deck.

The equation systems for the stability and vibration analyses are solved in the overlay BUCKLE. Subroutine BUCKLE is called for each value of the circumferential wave number N. The arrays derived in ARRAYS are read in from drum or disk.

If INDIC=1 (linear buckling analysis) the eigenvalue problem

$$(K_1+\lambda K_2+\lambda^2 K_3)\{x\}=0$$

is solved for the first NVEC eigenvalues with the correct sign (EBAND). In many structural systems, buckling is physically possible with loads of opposite sign than those actually present. Therefore, in EBAND eigenvalues that are negative are not counted as 'accepted' roots. It is possible, for example, for the user to specify NVEC=3 and for more than three eigenvalues to be obtained. The negative eigenvalues are given (printed out), and orthogonalizations are of course performed with respect to their associated eigenvectors; however, calculations will continue until the prescribed number (NVEC) of positive eigenvalues has been determined. With INDIC=2 the eigenvalue problem to be solved for NVEC eigenvalues is

$$(K_1-\Omega^2 M)\{x\}=0$$

in which M is the mass matrix. (M, incidentally, is not diagonal because u_i and v_i are at 'half' stations, and discrete ring rotatory inertia is included.) This solution occurs in subroutine EBAND2. The calculation of the lowest buckling load with nonlinear prebuckling effects included (INDIC$=-1$) is performed in EIGEN. Figure 16 summarizes the types of equations being solved for the various values of INDIC. All of these calculations (except for INDIC=3) are performed in Overlay BUCKLE.

The functions of the other two overlays MODE1 (MODE) and PLOT1 (PLOT) are given in Fig. 13.

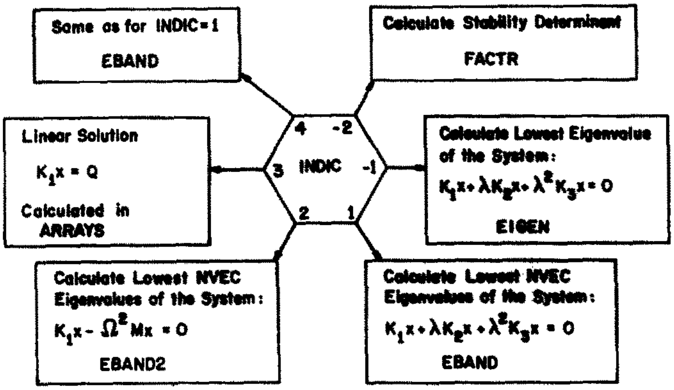

FIG. 16. Types of equations being solved for various INDIC.

ANALYTICAL RESULTS FROM BOSOR4

The remaining sections of the paper provide examples of the types of problems that BOSOR4 is designed to handle. The first seven examples are for shells of revolution, and the last two are for branched panels and columns. The first three and last two examples are from the BOSOR4 user's manual. The fourth, fifth, and sixth examples correspond to 'real-world' engineering problems. The seventh example represents an illustration of some of the problems involved in a buckling analysis in which nonlinear effects are important and in which eigenvalues are closely spaced. The examples are chosen to illustrate the seven types of analysis governed by the control integer INDIC. Computer times given in the text are for Univac 1108 double precision calculations on the EXEC8 system.

Example 1. *T-ring modeled as branched shell* (*INDIC*=1)

Figure 17 shows the discretized model and buckling loads predicted for a given range of circumferential waves N. BOSOR4 gives two minima in the range $2 \leq N \leq 16$. The minimum $N=2$ is a mode in which the cross-section does not deform—i.e. the ring ovalization mode. Buckling pressures calculated for this mode are very close to those computed from the well-known formula $q_{cr}=EI(N^2-1)/r_c^3$, in which q_{cr} is the critical line load in lb/in. (pressure integrated in the direction of segment 1), EI is the bending rigidity of the ring, and r_c is the radius to the ring centroidal axis. The minimum at about $N=11$ corresponds to buckling of the web. Approximately 20 sec of CPU time were required for this case.

Example 2. *Stress analysis of ring-stiffened cylinder with three-point loads* (*INDIC*=3)

Figure 18 presents the example with deflections and stresses shown schematically. The threepoint loads are modeled as a line load with three triangular 'pulses' applied to the ring. The results for stresses and displacements have apparently converged to a reasonably accurate value, since a 10-term Fourier expansion yields at $\theta=0$: $w=-0.000301$ in.,

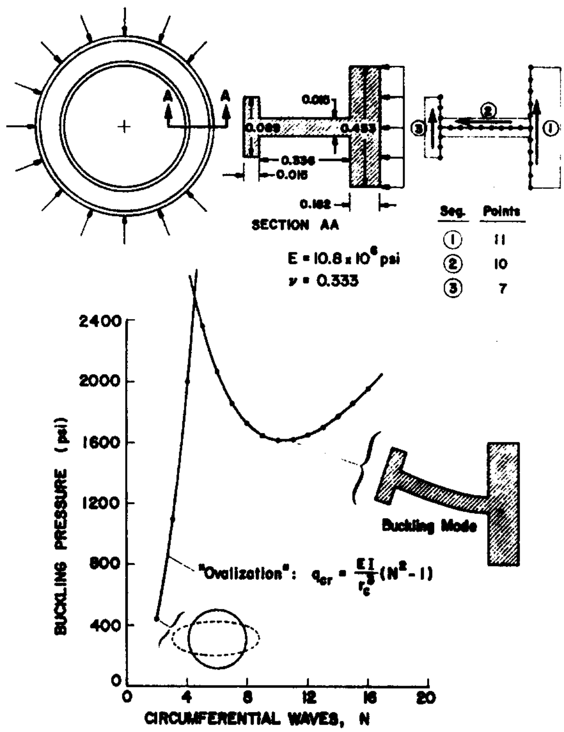

FIG. 17. Buckling of ring treated as branched shell.

σ_1 (outer)$=-6.19$ psi, and σ_2 (inner)$=6.02$ psi. Reduction of the number of points in the 40-in. length near the ring from 41 to 11 with use of 20 Fourier harmonics gives at $\theta=0$: $w=-0.000302$ in., σ_1 (outer)$=6.30$ psi, and σ_2 (inner)$=6.56$ psi. Similar small changes occur in the other variables. The reason that convergence with increasing number of Fourier harmonics is better than expected is that the ring essentially 'integrates' the applied load. It is for this reason that numerically one-dimensional shell-of-revolution codes based on Fourier superposition are frequently reliable and efficient for analysis of shell systems submitted to concentrated loads. The very rapid convergence with increasing number of mesh points in the short segment near the ring is a property of the finite-difference energy method, see Ref. [28]. Approximately 33 CPU sec on the 1108 were required for execution of the case described in Fig. 18. This includes time to plot six frames with about fifteen traces on each frame.

Example 3. *Buckling of conical shell heated on axial strip* (*INDIC*=4)

Figures 19 and 20 show the model and results. Figure 19 gives the temperature rise distribution at buckling as reported in Ref. [30]. Figure 20 shows the prebuckling stress and displacement distributions and the lowest three eigenvalues and eigenvectors corresponding to 20 circumferential waves. The eigenvalues denote a factor to be multiplied by the prebuckling temperature rise distribution. Twenty Fourier harmonics were used for the prebuckling analysis. The model consists of 309 degrees of freedom. A total of 74 sec of CPU time on the 1108 were required for execution of the case.

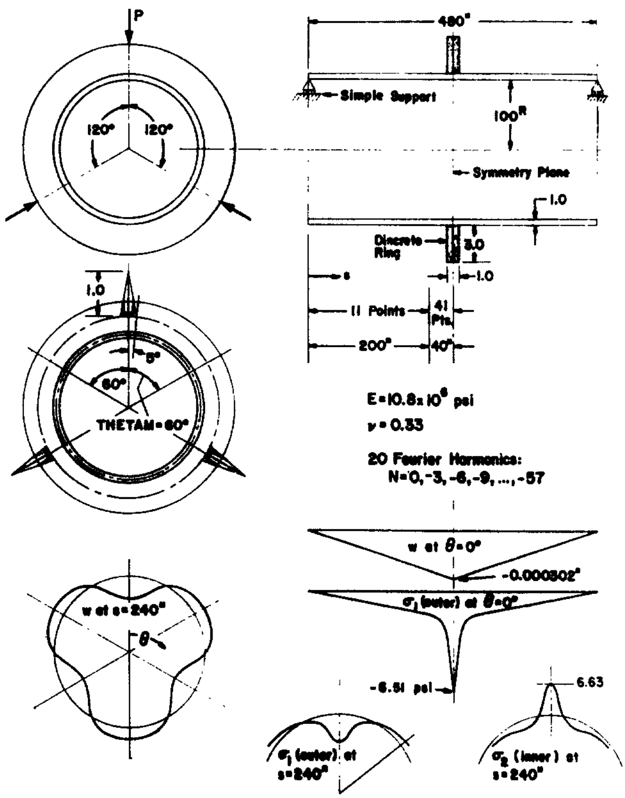

FIG. 18. Cylinder with three point loads.

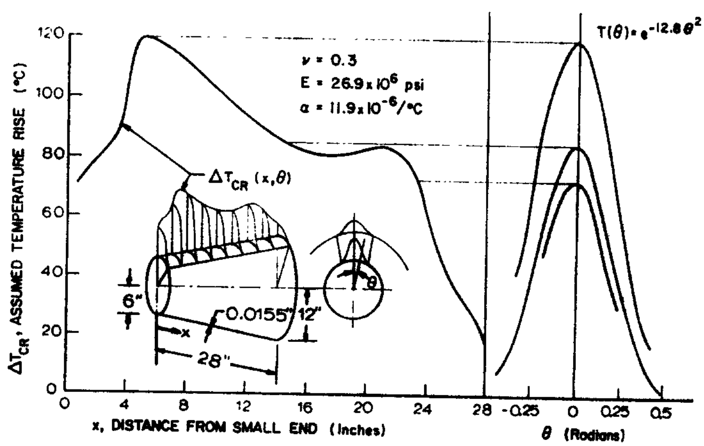

FIG. 19. Conical shell heated along axial strip.

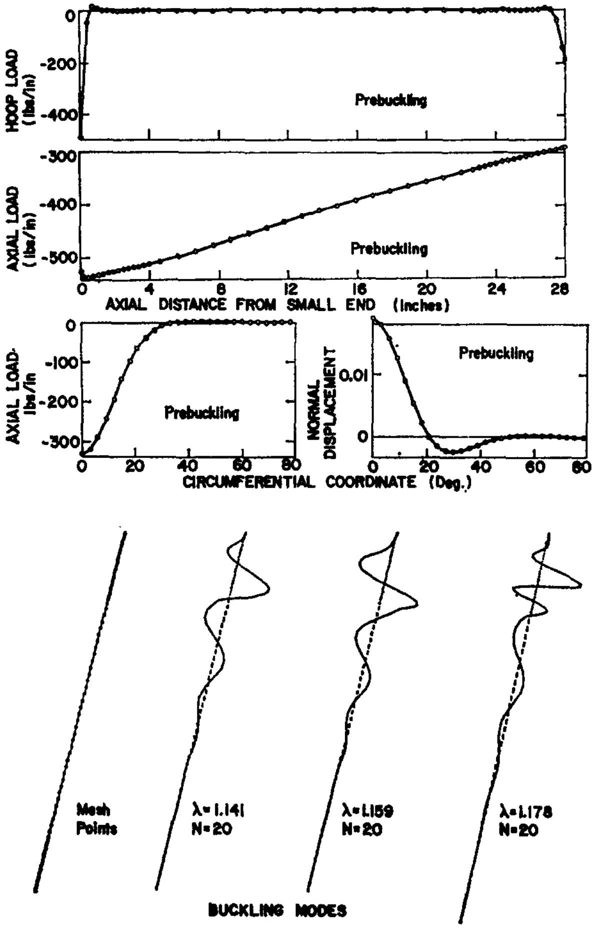

FIG. 20. Prebuckling state of heated cone and buckling modes.

Example 4. Buckling of a corrugated shroud under max. q nonsymmetric airloads (INDIC=4)

Figures 21–23 and Table 2 pertain to this case. Figure 21 gives SC4020 plots of the reference surface of the structure and some expanded views. Many of the ring stiffeners are treated as flexible shell structures. A discrete ring is shown as a centroid and an attachment point. Figure 22 shows details of how the modeling is done at a typical station. Figure 23 shows a schematic of the assumed pressure distribution, taken essentially from wind-tunnel data. Also shown in Fig. 23 are computer-generated plots of the prebuckling deformed structure and a buckling mode corresponding to the prestress distribution on the leeward (axially compressed) side of the shroud. Table 2 gives comparative computer times for various intermediate computations on the Univac 1108, IBM 370/165, and CDC 6600. The model consists of 1033 degrees-of-freedom with a stiffness matrix maximum semibandwidth of 133. Five Fourier harmonics were used for the prebuckling analysis.

TABLE 2. Buckling of nonsymmetrically loaded shroud—shroud analyzed as branched shell with 18 segments: 1033 degrees-of-freedom. Maximum semibandwidth: 133. 5 harmonics for stress analysis

		Computer Run Times (sec)				
Computations in process ([a]) (1108 and IBM 370 in double precision)	Circumferential waves	UNIVAC 1108 EXEC8 (CPU)	CDC 6600 FTN (OPT=1) Compiler (CPU)	CDC 6600 RUN Compiler (CPU)	IBM 370/165 (CPU)	IBM 370/165 Eigen values(d)
Read data and set up case	—	20.692	5.809	12.580	7.537	
Stiffness matrix K_{10} calculated	0	24.118	7.504	18.690	8.703	
$K_{10}x_0=Q_0$ solved and solution superposed on existing vectors at various meridional, circ. stations.	0	28.719	10.160	26.836	10.537	
Stiffness matrix K_{11} calculated	−1	32.335	11.859	32.930	11.720	
$K_{11}x_1=Q_1$ solved and solution superposed on existing vectors at various stations	−1	37.303	14.528	41.224	13.640	
Stiffness matrix K_{12} calculated	−2	40.780	16.216	47.320	14.847	
$K_{12}x_2=Q_2$ solved and solution superposed on existing vectors	−2	45.437	18.885	55.620	16.760	
Stiffness matrix K_{13} calculated	−3	48.914	20.578	61.714	17.907	
$K_{13}x_3=Q_3$ solved and solution superposed on existing vectors	−3	53.505	23.234	70.014	19.897	
Stiffness matrix K_{14} calculated	−4	56.971	24.941	76.110	21.083	
$K_{14}x_4=Q_4$ solved and solution superposed on existing vectors	−4	61.628	29.370	91.976	24.663	
Discrete ring loads and moments computed and superposed (29 rings) displacements and resultants printed	—	75.205	32.305	99.366	27.870	
Undeformed and deformed structure plotted		81.025	—(b)	—	—	
Begin buckling analysis:						
Stiffness matrix K_1 computed	13	85.689	34.291	106.760	29.147	
Load—geometric matrix K_2 computed	13	91.354	36.079	115.172	30.637	
Lambda—squared matrix K_3 computed	13	93.382	37.024	118.200	31.303	
Form $(K_1+MU_0{*}K_2+MU_0{*}MU_0{*}K_3)$($c$)	13	93.832	37.167	118.734	31.996	
Factor $K_1+MU_0{*}K_2+MU_0{*}MU_0{*}K_3$	13	98.096	39.555	126.064	33.556	
14 power iterations completed	13	118.824	46.592	157.942	44.296	3.64256
Shift $(K_1+MU_1{*}K_2+MU_1{*}MU_1{*}K_3)$, factor	13	123.600	49.102	165.710	46.566	
Six power iterations completed	13	132.017	52.128	179.408	51.373	3.64120
Shift $(K_1+MU_2{*}K_2+MU_2{*}MU_2{*}K_3)$, factor	13	136.367	54.631	187.178	53.563	
Three power iterations completed	13	140.741	56.156	195.190	55.986	3.64123
Calculate and store modal displacements	13	145.882	59.364	202.854	59.330	
Print and plot mode	13	149.654	−(b)	203.778	—	
Total CPU time (sec)		149.654	59.364	203.778	59.330	3.64123
Total I/O [see footnotes (e), (f), (g)]		15.0(e)	38.100(e)	1051(f)	(g)	

(a) 857 calls to subroutine GASP in this case. Each call to GASP causes data to be transferred from core to auxiliary mass storage or vice-versa.

(b) SC4020 plot software not available.

(c) MU_i = spectral shift by amount MU_i.

(d) Factor to be multiplied by pressure distribution shown in Fig. 23.

(e), (f) See footnotes (e), (f) in Table 3.

(g) See footnote (h) in Table 3.

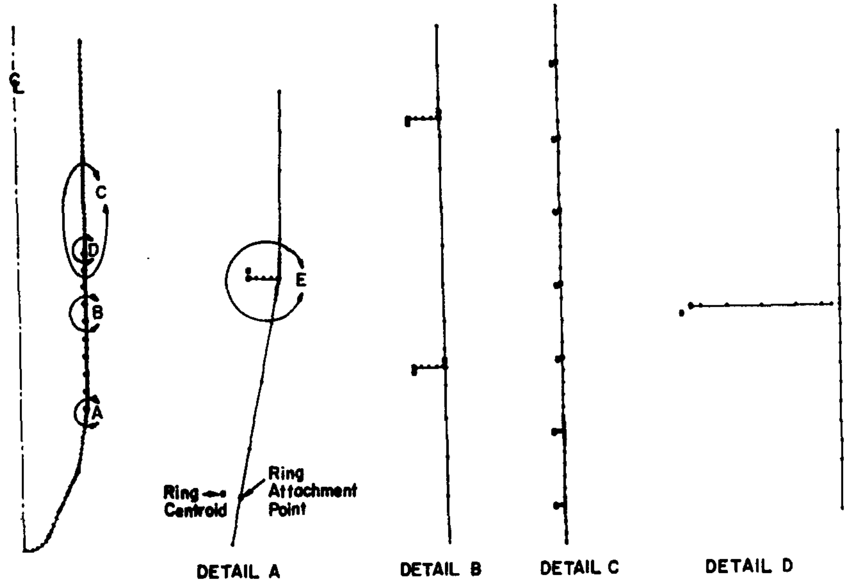

FIG. 21. Computer model of corrugated shroud with expanded views.

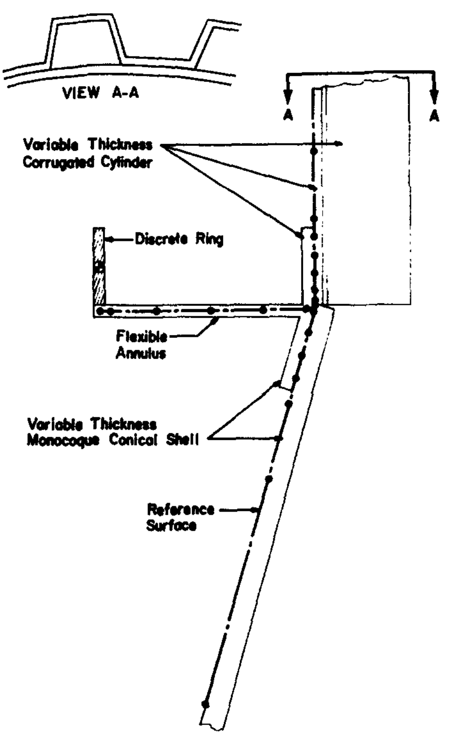

FIG. 22. Geometry of detail E of the shroud.

Example 5. Free vibration modes of a two-stage rocket ($INDIC=2$)

The model is shown in Fig. 24, and the vibration modes are depicted in Figs. 25 and 26. The rocket is considered to be empty, so that the modes do not contain the effects of fuel or payload. The first two modes for $N=0$ and $N=1$ circumferential waves are rigid-body modes. The first mode for $N=0$ is simply a rotation about the axis of revolution.

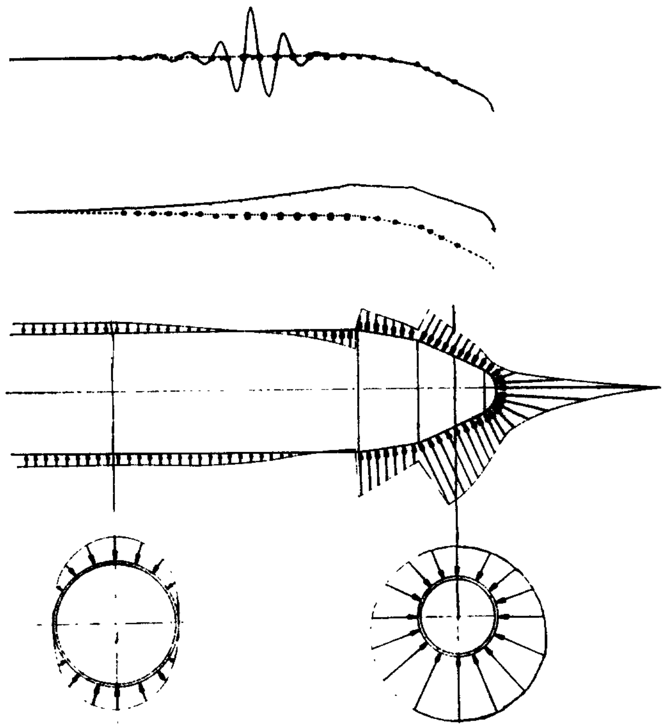

FIG. 23. Pressure distribution on the shroud, prebuckling deflection, buckling mode.

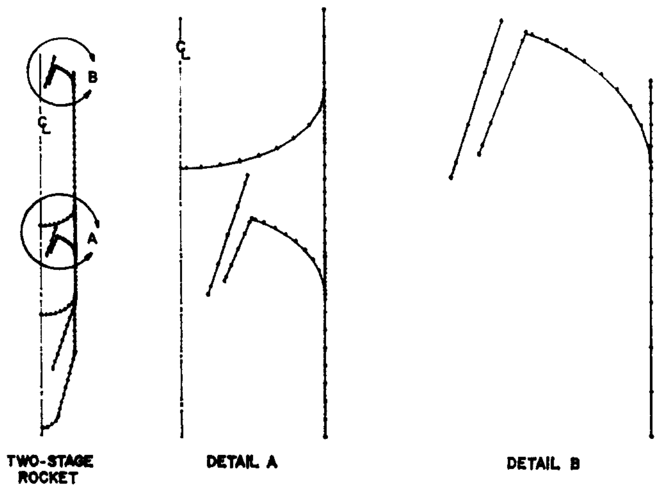

FIG. 24. Two-stage rocket: discretized model.

TABLE 3. Vibration of two-stage rocket treated as branched shell of 19 segments. Prestress analysis: 536 degrees-of-freedom. Vibration analysis: 784 degrees-of-freedom. Maximum semi-bandwidth in vibration analysis: 119, $N=2$ circumferential waves

Computations in process([a]) (1108 and IBM 370 in double precision)	Frequency (cps)	Computer Run Times (sec) UNIVAC 1108 EXEC-8 (CPU)	CDC 6600 FTN (OPT=1) Compiler (CPU)	CDC 6600 RUN Compiler (CPU)	IBM 370/165 (CPU)	IBM 370/165 Frequency (cps)
Read data and set up	—	11.810	3.049	3.310	4.710	
Prestress solution ($NR=1$)([b])	—	18.828	5.845	7.264	7.130	
Compute stiffness matrix K_1	—	21.557	7.216	9.298	8.050	
Compute mass matrix K_2	—	22.227	7.573	9.712	8.377	
Form $K_1-MU_1{*}K_2$ (shift)([c])	—	22.660	7.688	9.944	8.740	
Factor $K_1-MU_1{*}K_2$	—	24.904	8.964	11.746	9.543	
First power iteration completed	30.7808	25.594	9.219	12.176	9.883	27.4844
Second	27.1542	26.297	9.472	12.602	10.263	27.0189
Third	27.0698	26.991	9.722	13.028	10.603	27.0110
Fourth	27.0683	27.688	9.977	13.456	10.963	27.0082
Fifth	27.0653	28.380	10.227	13.882	11.340	27.0044
Thirteen more power iterations	27.0159	37.600	13.492	19.434	14.597	26.9738
Shift (Form $K_1-MU_2{*}K_2$)	—	37.756	13.532	19.486	14.860	—
Factor $K_1-MU_2{*}K_2$	—	40.058	14.808	21.286	15.643	—
14 power iterations completed([g])	26.8932	49.989	18.331	27.246	17.833	26.8685
Shift (form $K_1-MU_3{*}K_3$)	—	50.124	18.368	27.300	18.087	—
Factor $K_1-MU_3{*}K_2$	—	52.424	19.649	29.100	18.860	—
Five power iterations completed	26.8674	55.997	20.906	31.230	19.947	26.8676
Store mode shape on drum	—	56.012	20.910	31.234	19.950	—
Four power iterations, 2nd eigenvalue	27.2032	59.277	22.033	33.188	21.497	27.2031
Store mode shape on drum	—	59.297	22.039	33.192	21.500	—
Ten power iterations, 3rd eigenvalue	64,0898	67.111	24.832	37.918	25.673	64.0905
Shift (form $K_1-MU_4{*}K_2$) and factor	—	69.337	26.148	39.772	26.736	—
Four power iterations completed	64.0982	71.392	26.933	41.086	27.936	64.0983
Seven power iterations, 4th eigenvalue	82.6948	76.808	28.981	44.548	30.563	82.6942
Shift (form $K_1-MU_5{*}K_2$) and factor	—	79.082	30.302	46.398	31.533	—
Three power iterations completed	82.6958	81.189	31.092	47.724	32.683	82.6962
Seven power iterations, 5th eigenvalue	117.659	87.144	33.274	51.292	35.936	117.659
Shift (form $K_1-MU_6{*}K_2$) and factor	—	89.514	34.593	53.144	36.936	—
Three power iterations completed	117.657	91.693	35.392	54.486	38.096	117.657
14 power iterations for 6th eigenvalue	160.249	103.199	39.709	61.612	44.623	160.046
Shift (form $K_1-MU_7{*}K_2$) and factor	—	105.309	41.028	63.462	45.639	—
Four power iterations completed	160.086	108.167	42.089	65.242	47.166	160.085
Check if all roots found (shift again and factor and count)	—	110.567	43.421	67.116	48.919	—
Calculate and print out modes	—	119.363	45.945	69.776	52.089	—
Plot undeformed and deformed structure, modes (28 frames)	—	126.530	—(d)	—(d)	—(d)	—
Total CPU Time (seconds)		126.530	45.945	69.776	52.089	
Total I/O [see footnotes (e), (f), (h)]		13.000([e])	44.071([e])	1209([f])	(h)	

(a) 1029 calls to subroutine GASP in this case. Each call to GASP causes data to be transferred from core to auxiliary mass storage or vice-versa.
(b) NR means Newton–Raphson iterations.
(c) MU_i = spectral shift by amount MU_i.
(d) SC4020 plot software not available.
(e) This is 'equivalent' I/O sec as charged at the particular installation where cases run. For the CDC 6600 FTN case the actual I/O sec were about 100, but since the program required only 40 per cent of total core available, the charge (actual I/O sec) was 0.44 times the charge/(CPU-sec).
(f) This is the quantity of operating system (I/O) calls required at the NASA Langley CDC where this case was run. *Note*: Quantity of calls depends on the buffer size set by the user. 1500–3000 (decimal) is suggested.
(g) 6 power iterations required on IBM 370/165.
(h) I/O charge depends upon size of buffers and upon record lengths established in the JCL and in Subroutine GASP. As of 12/30/72 this aspect of the conversion of BOSOR4 to the IBM/370 had not been completed.

The two rigid-body modes for $N=1$ are orthogonal to each other, but are each linear combinations of a uniform lateral translation and rotation about the center of mass. The third mode for $N=0$ is localized in the neighborhoods of the nozzles, and expanded plots are given for clarification. Three of the modes involve local motion of the nozzles; the fourth mode for $N=1$ and the first and second modes for $N=2$. This vibration model contains 784 degrees of freedom and the maximum semibandwidth of the stiffness matrix is 119. Table 3 presents comparative data on computer CPU times for calculation of the six lowest eigenvalues for $N=2$ circumferential waves.

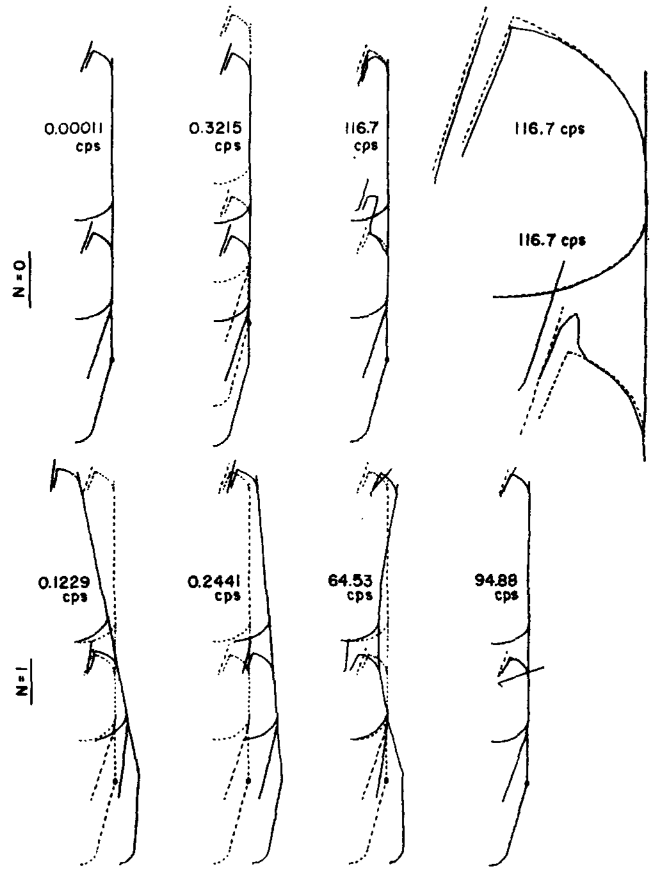

FIG. 25. Vibration modes for $N=0$ and $N=1$ waves.

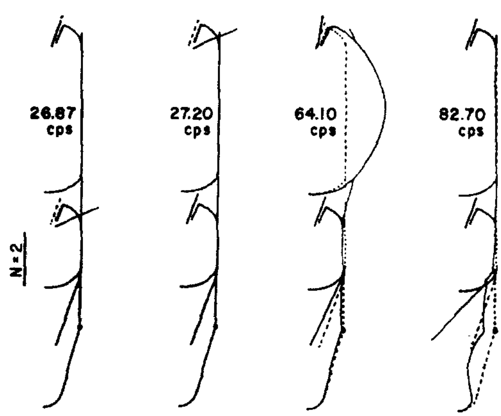

FIG. 26. Vibration modes for $N=2$ waves.

TABLE 4. Axially compressed cylinder treated as two segments. 83 points in edge zone segment, 99 points in other segment. Prebuckling analysis: 379 degrees-of-freedom. Stability analysis: 566 degrees-of-freedom.

Computations in Process ([a]) (1108 and IBM 370 in Double Precision)	Axial Load (lb/in.)	Circ. Waves (unitless)	Eigenvalue (unitless)	Computer Run Times (sec) UNIVAC 1108 EXEC-8 (CPU)	CDC 6600 FTN (OPT=1) Compiler (CPU)	CDC 6600 RUN Compiler (CPU)	IBM 370/165 (CPU)	IBM 370/165 Solutions
Read data and set up	0.0	0	—	5.844	1.724	1.862	2.640	
Prebuckling solution for L_1 ($NR=1$)([b])	0.0	0	—	8.886	2.836	3.590	3.513	
Prebuckling solution for $L_1+\Delta L$($NR=1$)	−1.0	0	—	11.709	3.951	5.322	4.470	
Compute stiffness matrix K_1	−1.0	15	—	13.952	5.122	7.056	5.193	
Compute load-geom. matrix, K_2	−1.0	15	—	16.634	6.183	9.025	6.047	
Compute lambda-squared matrix, K_3	−1.0	15	—	17.578	6.745	9.808	6.437	
Form $K_1+MU^*K_2+MU^*MU^*K_3$, start factoring	−1.0	15	—	17.761	6.793	9.876	6.660	
Factoring of shifted matrix K_{MU} done	−1.0	15	—	18.510	7.162	10.400	6.913	
First power iteration completed	−1.0	15	9627.7	19.008	7.353	10.744	7.180	−1736.1
Second	−1.0	15	16073.4	19.510	7.546	11.092	7.450	13691.9
Third	−1.0	15	16129.7	20.013	7.735	11.436	7.727	14212.8
Fourth	−1.0	15	15329.9	20.523	7.923	11.782	8.000	13838.9
Fifth	−1.0	15	14619.2	21.028	8.110	12.128	8.243	13535.9
Sixth	−1.0	15	13962.0	21.538	8.303	12.472	8.503	13307.7
Seventh	−1.0	15	13393.9	22.052	8.492	12.818	8.763	13131.3
Eighth	−1.0	15	12957.7	22.568	8.680	13.162	9.033	12992.9
Ninth	−1.0	15	12651.2	23.090	8.867	13.508	9.276	12883.0
Tenth	−1.0	15	12465.7	23.612	9.059	13.852	9.527	12794.9
Eleventh	−1.0	15	12349.4	24.123	9.249	14.198	9.807	12723.5
Shift (form $K_1+MU_1{}^*K_2+MU_1{}^*MU_1K_3$([c])	−1.0	15	—	24.771	9.475	14.594	10.347	
Factor shifted matrix	−1.0	15	—	25.465	9.846	15.118	10.627	
Eleven power iterations completed	−1.0	15	12213.3	31.228	11.930	19.252	13.700	12178.6
Shift (form $K_1+MU_2K_2+MU_2{}^*MU_2{}^*K_3$)	−1.0	15	—	31.843	12.155	19.310	14.203	
Factor shifted matrix	−1.0	15	—	32.537	12.524	19.836	14.503	
Eleven power iterations completed	−1.0	15	12156.9	38.418	14.606	24.186	17.640	12150.7
Shift (form $K_1+MU_3{}^*K_2+MU_3{}^*MU_3{}^*K_3$)	−1.0	15	—	39.114	14.834	not required	18.130	
Factor shifted matrix	−1.0	15	—	39.831	15.208	not required	18.407	
Six power iterations completed. Lowest eigenvalue has been obtained for load of −1.0lb/in. and 15 circular waves	−1.0	15	12147.4	44.390	16.933	not required	20.293	12147.4
K_1, K_2, and K_3 computed for $N=18$ waves	−1.0	18	—	50.507	19.753	28.698	23.076	
Four shifts, four factorings, and total of 42 power iterations for convergence	−1.0	18	12176.4	77.575	30.159	50.776	37.623	12178.8
K_1, K_2, and K_3 computed for 12 waves	−1.0	12	—	83,786	32,987	55.266	39.719	
Three shifts factorings; 35 power iterations	−1.0	12	12008.0	106.168	41.480	69.954	51.239	11983.0
K_1, K_2, and K_3 computed for 9 waves	−1.0	9	—	112.845	44.344	74.442	53.302	
Two shifts, factorings; 20 power iterations([e])	−1.0	9	12084.8	127.316	49.518	93.154	66.912	12133.5
Prebuckling solutions: $L_2=-12{,}008.0$ ($NR=6$)	−12008.0	0	—	136.460	53.293	98.964	69.938	−11983.0

Two shifts, factorings; 20 power iterations	−8422.4	[illegible]	[illegible]	[illegible]	[illegible]	[illegible]	[illegible]	
K_1, K_2, and K_3 computed for 18 waves	−8422.4	18	—	227.935	90.954	160.510	104.847	− 8404.9
Two-shifts, factorings; 17 power iterations	−8422.4	18	284.867	239.268	95.571	168.412	112.190	288.278
K_1, K_2, and K_3 computed for 21 waves	−8422.4	21	—	245.216	98.371	172.902	114.084	− 8404.9
Two shifts, factorings; 18 power iterations(f)	−8422.4	21	326.366	257.560	103.194	181.490	117.217	329.960
Prebuckling solution: $L_4 = L_3 + 284.867{*}L_3/1000$ ($NR=4$)	−10809.0	0	—	264.539	105.902	185.668	119.313	−10814.6
Prebuckling solution for $L_4 + L_4/1000$ ($NR=1$)	−10819.2	0	—	267.384	107.015	187.402	120.200	−10825.4
K_1, K_2, and K_3 computed for 18 waves	−10819.2	18	—	273.423	109.807	191.900	122.203	−10825.4
Two shifts, factorings; 16 power iterations	−10819.2	18	−39.7476	285.308	114.440	199.830	128.560	−40.1023
Prebuckling solution: $L_5 = L_4 - 39.7476{*}L_4/1000$ ($NR=3$)	−10379.0	0	—	290.624	116.602	203.200	130.276	−10380.9
Prebuckling solution for $L_5 + L_5/1000$ ($NR=1$)	−10389.4	0	—	293.571	117.720	204.930	131.316	−10391.3
K_1, K_2, and K_3 computed for 18 waves	−10389.4	18	—	299.978	120.515	209.420	133.293	−10391.3
One shift, factoring; 4 power iterations	−10389.4	18	−10.1398	304.499	122.266	212.278	135.643	−10.4198
Prebuckling solution: $L_6 = L_5 - 10.1398{*}L_5/1000$ ($NR=2$)	−10273.7	0	—	308.923	123.881	214.828	137.013	−10272.7
Prebuckling solution for $L_6 + L_6/1000$ ($NR=1$)	−10283.9	0	—	311.889	124.968	216.556	137.972	−10283.0
K_1, K_2, and K_3 computed for 18 waves	−10283.9	18	—	318.365	127.685	221.040	139.956	−10283.0
One shift, factoring; 3 power iterations	−10283.9	18	−0.4033	322.173	129.191	223.552	142.143	− 0.4239
Print and plot mode shape, prebuckling mode, Undeformed and deformed structure	−10283.9	18	—			224.394	143.179	−10283.0
Total CPU time (sec)				326.854	129.961	224.394	143.179	
Total I/O [see footnotes (g), (h) and (i)]				25·8(g)	120.0(g)	3202(h)	(i)	

(a) 2982 calls to subroutine GASP in this case. Each call to GASP causes data to be transferred from core to mass storage or vice versa.

(b) NR means Newton–Raphson iterations.

(c) MU_i = spectral shift by amount MU_i.

(d) UNIVAC 1108 solutions. CDC 6600 and IBM 370 give slightly different results because of different initial random vector in power iteration method.

(e) IBM 370 run required 3 shifts, factorings and 36 power iterations.

(f) IBM 370 run required 1 shift, factoring and 8 power iterations.

(g), (h), (i) See footnotes (e), (f), and (h) in Table 3.

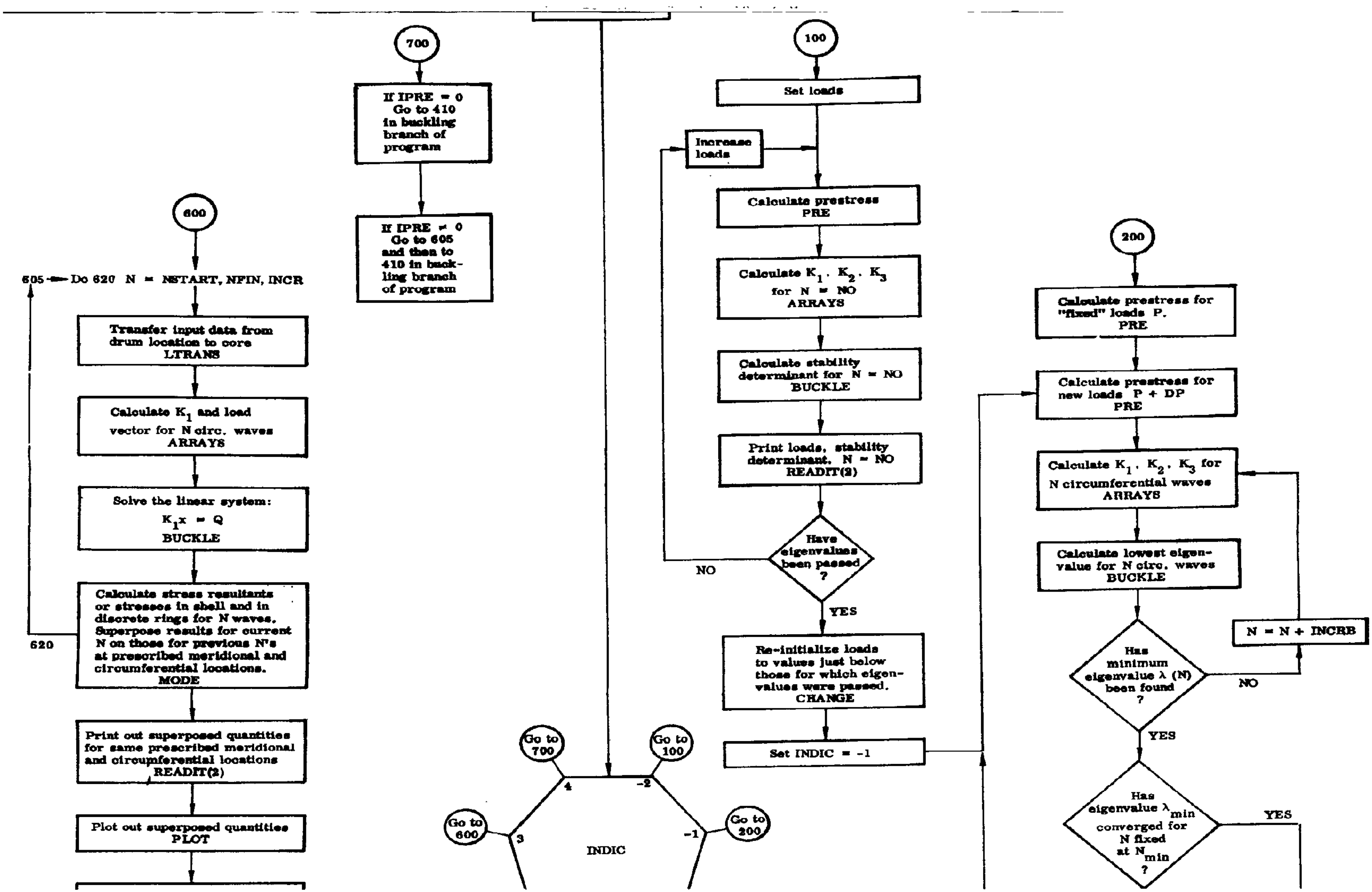

700
If IPRE = 0 Go to 410 in buckling branch of program
If IPRE ≠ 0 Go to 605 and then to 410 in buckling branch of program
600
605 Do 620 N = NSTART, NFIN, INCR
Transfer input data from drum location to core LTRANS
Calculate K1 and load vector for N circ. waves ARRAYS
Solve the linear system: K1x = Q BUCKLE
Calculate stress resultants or stresses in shell and in discrete rings for N waves. Superpose results for current N on those for previous N's at prescribed meridional and circumferential locations. MODE
620
Print out superposed quantities for same prescribed meridional and circumferential locations READIT(2)
Plot out superposed quantities PLOT
Go to 700
Go to 100
Go to 600
Go to 200
4
-2
3
-1
INDIC
100
Set loads
Increase loads
Calculate prestress PRE
Calculate K1, K2, K3 for N = NO ARRAYS
Calculate stability determinant for N = NO BUCKLE
Print loads, stability determinant, N = NO READIT(2)
Have eigenvalues been passed ?
NO
YES
Re-initialize loads to values just below those for which eigenvalues were passed. CHANGE
Set INDIC = -1
200
Calculate prestress for "fixed" loads P. PRE
Calculate prestress for new loads P + DP PRE
Calculate K1, K2, K3 for N circumferential waves ARRAYS
Calculate lowest eigenvalue for N circ. waves BUCKLE
Has minimum eigenvalue λ (N) been found ?
NO
N = N + INCRB
YES
Has eigenvalue λmin converged for N fixed at Nmin ?
YES

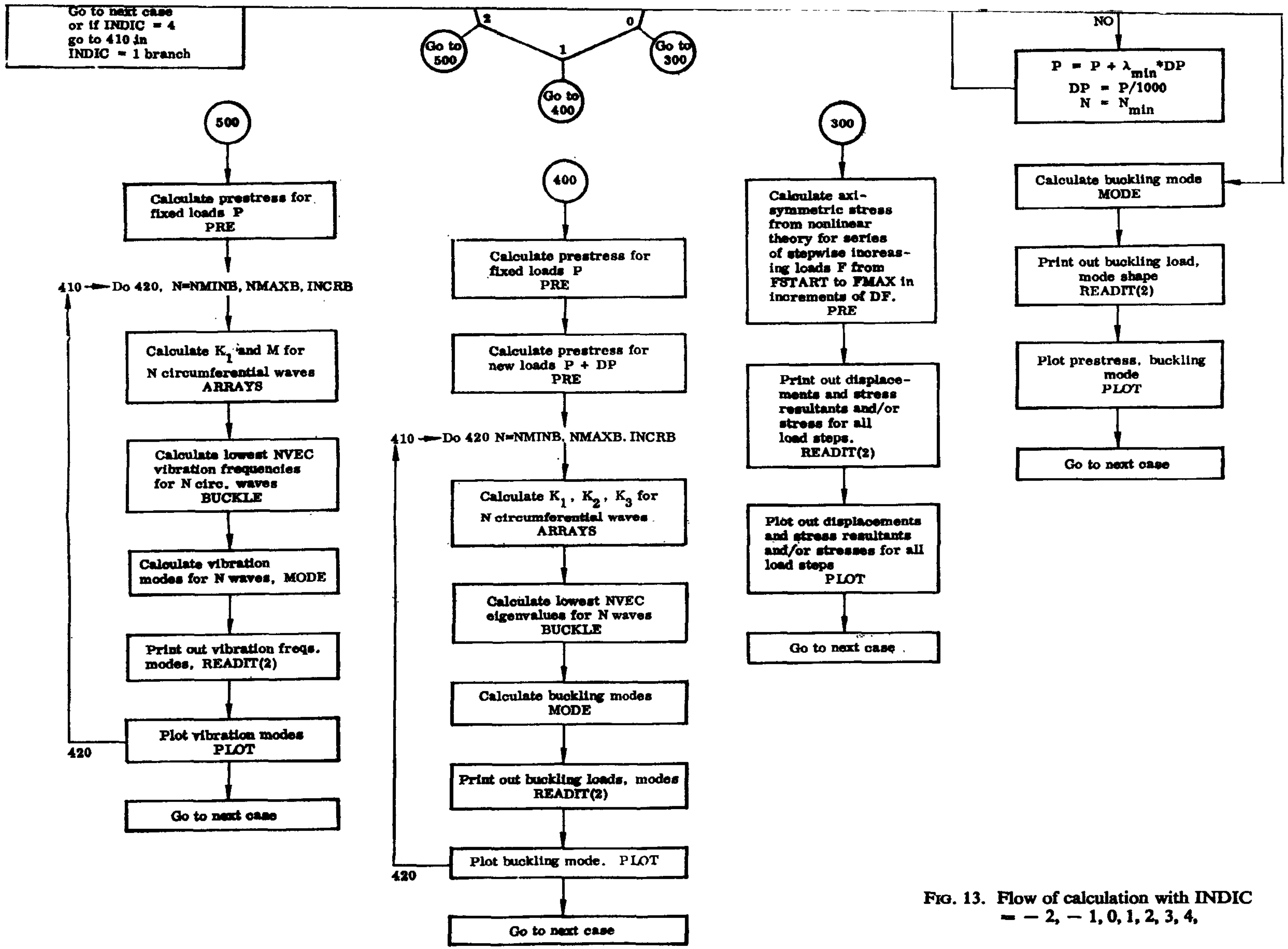

FIG. 13. Flow of calculation with INDIC = − 2, − 1, 0, 1, 2, 3, 4,

Example 6. Failure of a ring-reinforced cylinder under hydrostatic external pressure (INDIC =1, −1, −2, and 0)

In this model, shown in some detail in Fig. 27, the slender webs are treated as flexible annuli and the flanges as discrete rings. The problem is a good illustration of a typical sequence of computer runs that might be required for analysis of a complex shell of revolution where several failure modes are possible.

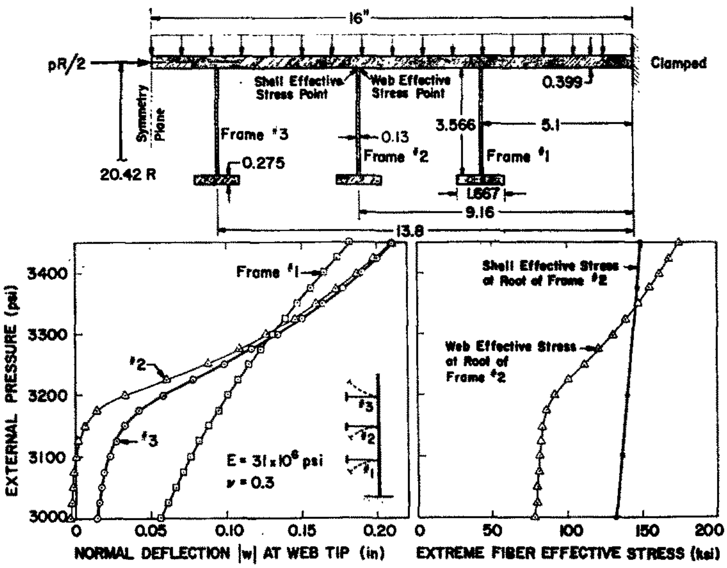

FIG. 27. Nonlinear stress analysis of frame-reinforced cylinder.

The choice of INDIC=1 for a preliminary analysis is logical because one suspects that buckling may be the primary mode of failure, and with INDIC=1 one can obtain approximate buckling pressures for a wide range of circumferential wave numbers without too large an expenditure for computer time. The initial choice of INDIC=1 is particularly appropriate in this case because it is apparent that more than one minimum buckling pressure exists in the $p_{cr}(N)$ vs N space: The shell may buckle axisymmetrically through 'sidesway' of the deep ring stiffeners; it may buckle nonsymmetrically in a low-N general instability mode in which cylinder and rings move together; it may buckle nonsymmetrically in a higher-N 'panel' or 'bay' mode in which the rings are located at displacement nodes in the buckle pattern; or the webs of the rings may buckle nonsymmetrically in a still-higher N mode similar to that shown in Fig. 17. The choice of INDIC=1 with a wide range of N would reveal all of these modes and cause to be calculated approximate critical pressures corresponding to them. The top insert in Fig. 28 shows the results of such an analysis. The lowest minimum corresponds to axisymmetric bifurcation buckling ('sidesway' of the webs).

Suppose that bifurcation buckling loads have been calculated from the INDIC=1 branch of BOSOR4 and the minimum critical pressure has been determined approximately from linear theory. The user should now check the accuracy of this prediction by choosing INDIC=−1 (nonlinear prebuckling effects). In this case, however, the INDIC=−1 branch does not succeed in finding an eigenvalue corresponding to N=0. It is necessary

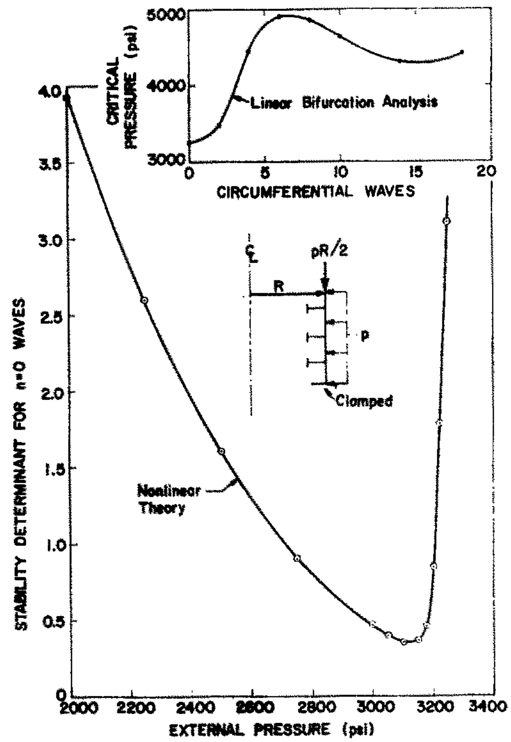

FIG. 28. Linear (INDIC=1) and nonlinear (INDIC=−2) bifurcation buckling analyses of frame-reinforced cylinder.

to choose INDIC=−2 ('plot' stability determinant) to find out why. Figure 28 shows results of the INDIC=−2 analysis. At a pressure close to the bifurcation pressure with INDIC=1, the stability determinant changes direction rather abruptly, indicating fairly large changes in prebuckling deformations for small changes in pressure. Since the stability determinant does not change sign, it is not surprising that the INDIC=−1 branch fails to find an eigenvalue. A final computer run with INDIC=0 gives axisymmetric nonlinear displacements and stresses for increasing pressure. The results of the INDIC=0 analysis are shown in Fig. 27. The rather abrupt increase in rate of 'sidesway' in frames No. 2 and No. 3 bectween 3,100 and 3,200 psi is the cause of the change in direction of the stability determinant shown in Fig. 28. Failure of the structure would probably occur at the root of frames No. 2 or No. 3 because of high (and rapidly increasing) stresses there.

Example 7. Buckling of very thin cylinder under axial compression (INDIC=−1)

This example is included because nonlinear prebuckling effects are fairly important; it is a difficult case from a numerical point of view, since eigenvalues are close together and close to the axisymmetric collapse load; and the case demonstrates some of the internal checks and automatic internal control in BOSOR4. Because of these properties it is one of the cases that a previous program, the BOSOR3, could not handle very well.

Figure 29 shows the model of a cylinder with radius R=500 in., thickness t=1in., length L=2,000 in., Young's modulus $E=10^7$ psi and Poisson's ratio ν=0.3. The cylinder is treated as being symmetric about the midlength, and the 1,000-in. half-cylinder thus analyzed is divided into two segments: a 200-in.-long edge zone segment with 83 mesh

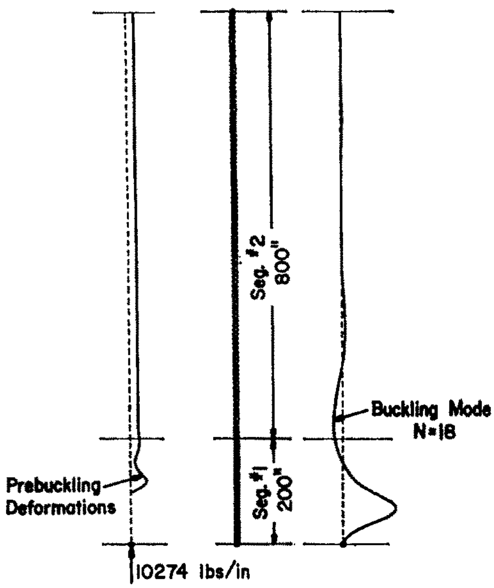

FIG. 29. Buckling of axially compressed cylinder.

points, and an 800-in.-long interior segment with 99 mesh points. The axisymmetric prestress model thus contains 379 degrees-of-freedom, and the stability model 566 degrees-of-freedom. Simple support conditions are applied at the edge, and symmetry conditions at the midlength. Also shown in Fig. 29 are the prebuckling displacement distribution at the predicted critical load of 10,274 lb/in. and the buckling mode corresponding to $N=18$ circumferential waves.

With the INDIC$=-1$ option the user supplies a starting load, a starting range of N, and an initial value of N. Through a sequence of operations the program first searches for an approximate local minimum buckling axial load $V_{cr}(N)$ within the given range of N. Once the N corresponding to the approximate minimum V_{cr} has bee found, N becomes fixed and a sequence of eigenvalue problems is established through which a final accurate buckling load is computed at that value of N with nonlinear prebuckling effects accounted for.

Figure 30 shows the sequence of wave numbers and loads automatically explored by BOSOR4 to obtain the final result $L_6=V_{cr}=10{,}274$ lb/in. With an initial base or 'fixed' load of 0 and a 'variable' load (quantity to be multiplied by eigenvalue) of 1.0 lb/in., eigenvalues labeled (1), (2), (3), and (4) are calculated. The base or 'fixed' load is then set equal to the local minimum or 12,008 lb/in. The 'variable' or 'eigenvalue' load is set equal to 12,008/1,000 lb/in. The small increment over a relatively large fixed value gives an accurate approximation of the 'local' rate of change of prebuckling stresses and rotations with load–local change about a given base or 'fixed' point. This technique permits formulation of another eigenvalue problem analogous to that represented by equation (1), in which K_1 is the stiffness matrix for $N=12$ waves, including the effects of the 'fixed' preload $L_2=12{,}008$ lb/in., and K_2 and K_3 are the load-geometric and lambda-squared matrices. These matrices depend on various parameters as well as on the differences between the prebuckling stress resultants and rotations at the 'fixed' load and those at the load $L_2+L_2/1{,}000$. For this problem, the eigenvalue λ is the factor that, when multiplied

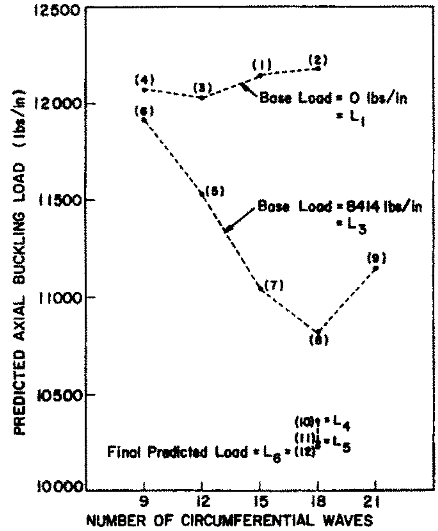

FIG. 30. Sequence of axial load and circumferential wave number estimates during calculation of buckling of cylinder with nonlinear prebuckling effects included.

by the load difference $L_2/1,000$, gives the quantity that must be added to the base or 'fixed' load $L_2=12,008$ to give a new base load. A third eigenvalue problem at $N=12$ can then be set up corresponding to the new base load. Ordinarily, calculations would continue in this manner until λ is smaller than a certain prescribed amount.

In this case, however, it is determined by BOSOR4 that for $N=12$ circumferential waves, three eigenvalues exist below the 'fixed' load 12,008 lb/in. Hence, the load is automatically reduced by a factor of 0.7 to 8,414 lb/in. With the eigenvalues corresponding to points 5, 6, 7 and 8 and 9 in Fig. 30 determined, the new base load $L_3=10,819$ lb/in. is established corresponding to $N=18$ waves. It is also determined by BOSOR4 that at $N=18$ one eigenvalue exists below this new base load. However, the new load need not be reduced by some factor because initial inverse power iterations for the eigenvalue nearest to $L_3=10,819$ indicate that subsequent critical load estimates will further reduce the base loads L_4, L_5, etc., to the lowest eigenvalue rather than increase them toward the second eigenvalue. Figure 30 shows the final three load estimates, L_4, L_5, and L_6.

Table 4 identifies various computations and gives current 'fixed' loads, circumferential wave numbers, eigenvalues, and CPU computer times. Underlined eigenvalues represent values to which the inverse power iterations with spectral shifts converge. This particular case requires much more than the average computer time for a nonlinear buckling analysis with the same number of degrees of freedom for the following reasons:

(1) The eigenvalues for each N are closely spaced, so that many inverse power iterations and spectral shifts are required for convergence.

(2) The eigenvalues are close to the axisymmetric collapse load of the cylinder. Rapidly changing nonlinear behavior in the neighborhood of the eigenvalues causes the requirement for more than the average number of base loads (L_1–L_6) with associated reformulations of the eigenvalue problem.

Figure 31 shows the prebuckling load deflection curve for this cylinder. The abscissa represents the difference between the actual end shortening and the end shortening that would exist if there were no prebuckling rotations. Eigenvalues computed with the INDIC $=+1$ branch for $N=18$ waves are shown as crosses. Several runs were made, each run corresponding to a different base or 'fixed' load. The open circles correspond to the various base loads, L_i. The large dots represent the 'fixed' loads used in the sequence shown in Fig. 30. Two to four eigenvalues are calculated corresponding to each open-circle base

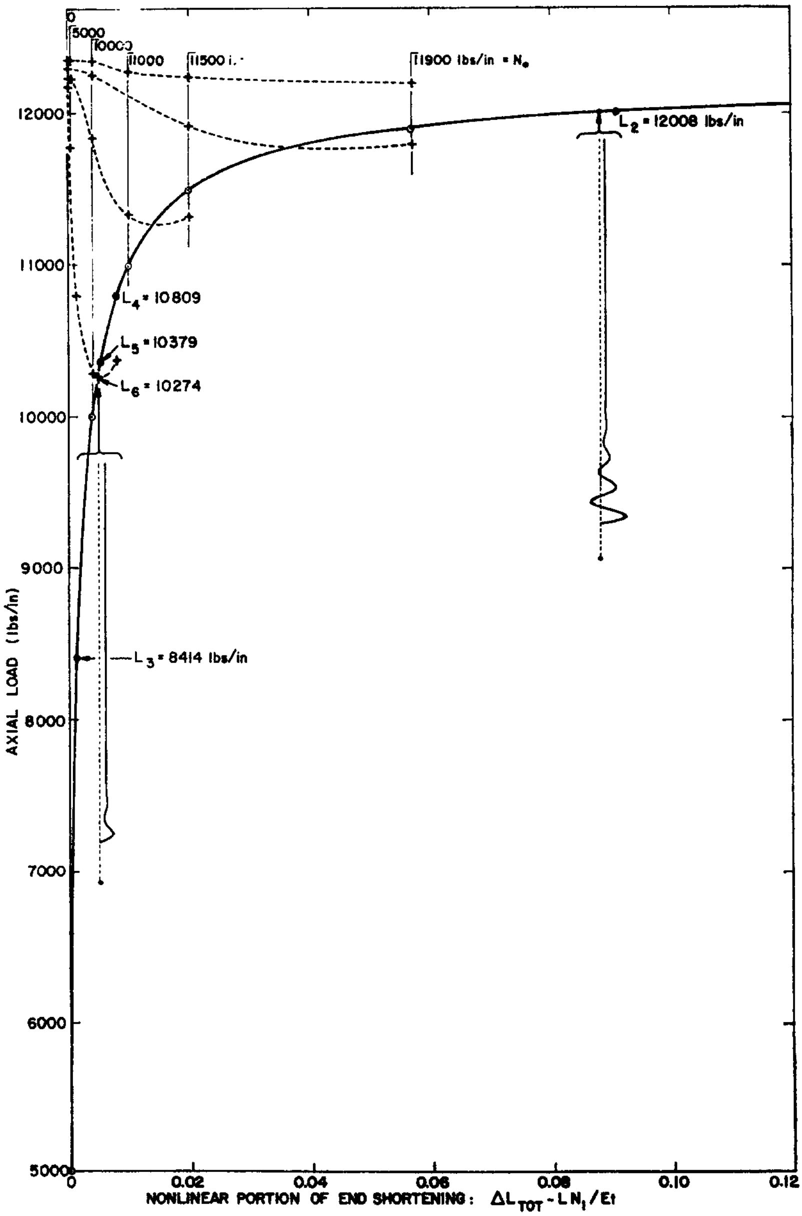

FIG. 31. Eigenvalue 'separation' for axially compressed cylinder.

load. These eigenvalues are indicated by crosses on the same vertical lines as the open circles. The eigenvectors are shown in Fig. 32. Notice that for 'fixed' load $L=0$, the lowest four eigenvalues are very close and are all approximately equal to the 'classical' load $0.605\ Et^2/R$. The lowest eigenvalues are also close for $N=15$. It is apparent from Table 4 that several inverse power iterations and spectral shifts are required to obtain the lowest eigenvalue at that wave number. A total of 39 inverse power iterations and four spectral shifts are required for convergence to the lowest eigenvalue. For $L=5{,}000$ lb/in. the lowest eigenvalue 'separates' from the others, and the localized nature of the corresponding eigenvector is strongly developed (Fig. 32). Because of this separation of the lowest eigenvalue, fewer inverse power iterations and spectral shifts are required for convergence. From Table 4 for $N=15$ and 'fixed' load $L_3=8{,}422$ lb/in. it is seen that a total of twenty power iterations and two spectral shifts are required. Thus, the user may save considerable computer time by choosing a base or 'fixed' load to be some reasonable percentage of the estimated final buckling load. This is particularly true if many values of the wave number N are to be explored and if the predicted N corresponding to minimum $V_{cr}(N)$ is likely to depend strongly on the fixed portion of the load, as is the case for axially compressed very thin cylinders.

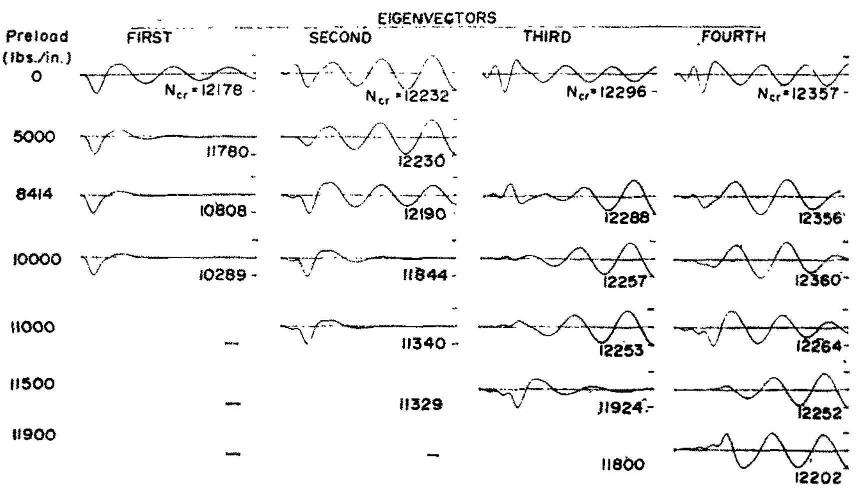

FIG. 32. Eigenvectors and eigenvalues for axially compressed cylinder with various base loads.

STRESS, BUCKLING AND VIBRATION OF PRISMATIC SHELL STRUCTURES

An interesting and not immediately obvious use of BOSOR4 is for buckling and vibration analysis of prismatic shell structures, in particular composite branched panels. This technique of using a shell-of-revolution program for the treatment of structures that are not axisymmetric is discussed in detail in Ref. [25]. Figure 33, reprinted from that article, shows various types of prismatic shell structures that can be handled by BOSOR4. Examples involving stress and buckling of oval cylinders, cylinders with nonuniform loads, and corrugated and beaded panels are given in Ref. [25] as well as a study of vibration of a stringer-stiffened shell in which the stringers are treated as discrete. In the analysis of buckling of nonuniformly loaded cylinders, the nonsymmetry of the prestress can be accounted for in the stability analysis. In BOSOR4 the capability described in Ref. [25] is extended to branched prismatic shell structures.

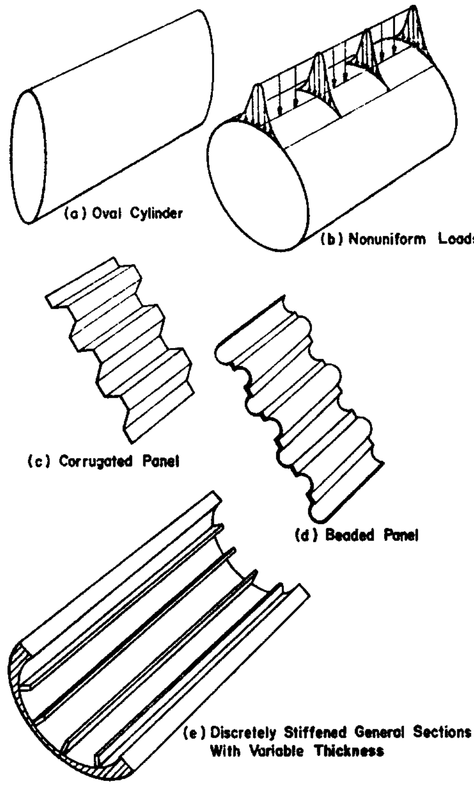

FIG. 33. Some prismatic shell structures that can be analyzed with use of BOSOR4.

Example 8. *Axially compressed semi-sandwich corrugated panels* (*INDIC*=4)

Figure 34 shows two types of semisandwich corrugated construction, bonded and riveted. The panels are treated as giant annuli with mean radius of 2,750 in. and outer radius minus inner radius equal to about 7.4 in. Both panels are assumed to carry an axial compressive stress (panels loaded normal to plane of figure) that is constant along the axis of the panel and over all of the little segments shown at the top of Fig. 34. In the model on the left-hand side of the figure the troughs of the corrugated sheet and the flat skin are assumed to be united by a perfect bond of zero thickness. The thickness of the panel in these areas is equal to the sum of the thickness of the flat sheet and the corrugated sheet. In the riveted panel the displacements and rotations of the corrugated sheet are constrained to be equal to those of the flat skin only at the midlengths of the troughs, thus simulating a rivet of zero diameter in the plane of the paper and continuous in the direction normal to the plane of the paper. The computer-generated plots show the undeformed and deformed panels for buckling modes with various wave lengths L in the direction normal to the plane of the paper. The riveted panel is weaker in axial compression because the rivets permit more local distortion of the cross-section than does the continuous bonding. The modes shown are more or less general instability modes. One can calculate buckling loads for much shorter L, such as L=1.0 in., in order to determine the effect of method of fastening on crippling loads.

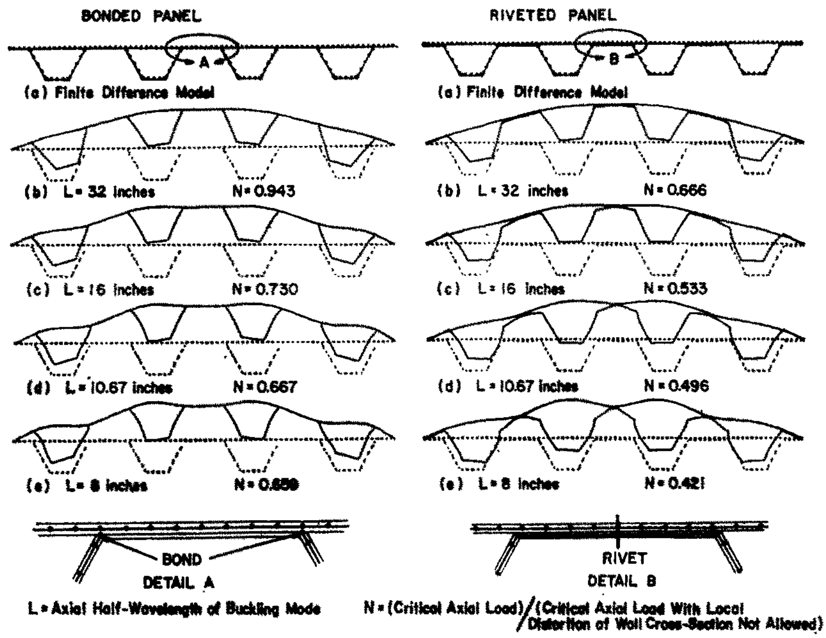

FIG. 34. Buckling modes of axially compressed semisandwich bonded and riveted corrugated panels.

Example 9. Buckling of an axially compressed branched, composite column (INDIC=4)

Figure 35 shows a cross-section of the column submitted to uniform compressive shortening normal to the plane of the paper. The column is made of aluminium, and the

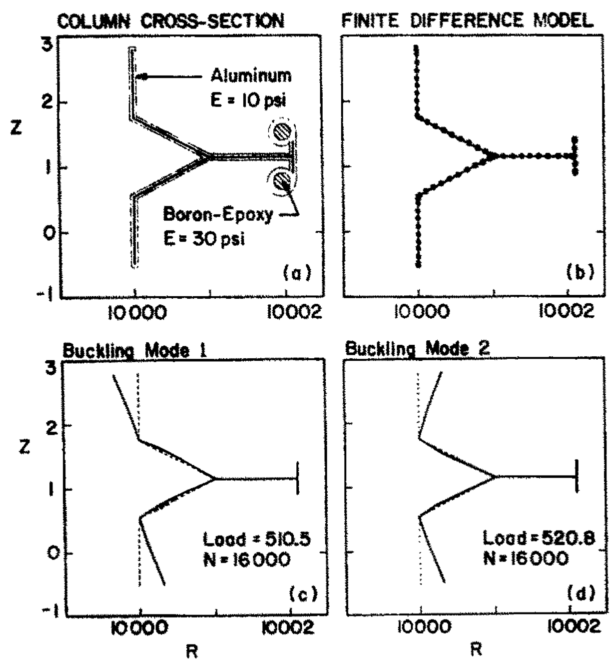

FIG. 35. Buckling of branched composite column under axial compression (load normal to plane of paper).

circular appendages attached to the short flange are filled with boron epoxy composite. The column is treated as a shell of revolution, with radius from the axis of revolution to the two 'foot' flanges equal to 10,000 in. The mesh-point distribution is shown in Fig. 35b, and two buckling modes corresponding to an axial half-wavelength of $10{,}000 \times \pi/N = 1.96$ in. are shown in Fig. 35c and d. These modes represent antisymmetric and symmetric crippling of the foot flanges. The critical 'loads' 510.5 and 520.8 are actually eigenvalues, quantities to be multiplied by the loads per length along the cross-section of the column, which for this INDIC=4 run are read from cards as input data.

SUMMARY

The paper gives a complete description of the BOSOR4 computer program, which runs on the CDC 6600, UNIVAC 1108, and IBM 370/165 computers. The literature on computer programs for shells and solids of revolution is briefly reviewed. BOSOR4 and other computer programs are shown in a 'capability' chart. The basic assumption upon which BOSOR4 rests are enumerated, and the finite-difference energy method is described. The formulation of the stability problem is shown, and the strategy is demonstrated for obtaining the lowest buckling load in cases for which the eigenvalues are closely spaced and the problem is highly nonlinear at loads in the neighborhood of the bifurcation buckling. Examples of stiffness matrices for branched systems of shells are shown. Overlay charts with required core storage are given for operation of BOSOR4 on the CDC6600, UNIVAC 1108, and IBM 370/165. A schematic of a typical data deck is shown. Flow charts are given for the seven types of analysis that BOSOR4 will perform: buckling with nonlinear prebuckling, nonlinear axisymmetric stress, buckling with linear prebuckling, vibration with nonlinear axisymmetric prestress, linear nonsymmetric stress with automatic calculation of Fourier series of nonsymmetric loads and automatic superposition of harmonics, buckling with linear nonsymmetric prestress, and calculation of stability determinant for an increasing sequence of applied loads. Examples are given for each of these types of analysis with central processor times given on the CDC, UNIVAC, and IBM computers for the various operations during the execution of three typical rather large cases. The use of BOSOR4 for the calculation of buckling loads of branched, prismatic shell structures such as a semi-sandwich corrugated panel is demonstrated.

Acknowledgements—The author is indebted to Frank Brogan, Tom Peterson, Chet Dyche, Bo Almroth, Bill Loden, and Rod Kure, who wrote some of the subroutines used in the BOSOR4 program. Particular appreciation is expressed for the many fruitful discussions with Frank Brogan and Bo Almroth concerning the numerical aspects of the analysis, and with Jörgen Skogh about ways in which to make the BOSOR4 program easy to use. The author is thankful also for Frank Brogan's assistance in the conversion of BOSOR4 for operation on the CDC 6600 and Tom Peterson's, Pete Smolenski's, and Bob Mitchell's assistance in the conversion for operation on the IBM 370/165.

The development of BOSOR4 was sponsored by the Department of Structural Mechanics of the Naval Ship Research and Development Center under Naval Ship Systems Command, Operation and Maintenance Navy Fund, Contract N00014-71-C-0002. Rembert Jones and Joan Roderick were technical monitors. The work involved in converting BOSOR4 for operation on the CDC 6600 was sponsored by the NASA Langley Research Center, Contract NASI-10929, with Paul Cooper as technical monitor.

Some of the numerical studies were performed under the Lockheed Missiles & Space Company's Independent Research Program.

REFERENCES

[1] D. Bushnell, Stress, stability, and vibration of complex branched shells of revolution. *Analysis and User's Manual for* BOSOR4. Lockheed Missiles & Space Company, Inc., LMSC-D243605, Sunnyvale, California (March 1972). Also NASA CR-2116 October (1972).

[2] G. A. Cohen, Computer analysis of ring-stiffened shells of revolution. Langley Research Center, NASA CR2085, Hampton, Virginia, September (1972).

[3] A. P. CAPPELLI, T. S. NISHIMOTO and P. P. RADKOWSKI, The analysis of shells of revolution having arbitrary stiffness distribution. *Proc. AIAA/ASME 8th Structures, Structural Dynamics and Materials Conference*, pp. 732–749, Palm Springs, California, (1967).
[4] R. M. JONES and J. G. CROSE, SAAS II, finite element stress analysis of axisymmetric solids with orthotropic, temperature-dependent material properties. TR-0200 (S4980)-1, SAMSO TR-68-455, Aerospace Corporation, San Bernardino, California, September (1968).
[5] N. A. CYR and R. D. TETER, Finite element elastic-plastic-creep analysis of two-dimensional continuum with temperature-dependent material properties. *National Symposium on Computerized Structural Analysis and Design*, George Washington University, Washington, D.C., 27–29 March (1972).
[6] M. B. MARLOWE, *FARSS User's Manual*. Fourier analysis of rotationally symmetric solids. Lockheed Missiles & Space Company, Inc., Sunnyvale, California, Report (1972).
[7] S. GHOSH and E. L. WILSON, Dynamic stress analysis of axisymmetric structures under arbitrary loading. Earthquake Engineering Research Center, Report EERC 69-10, University of California, Berkeley, California, September (1969).
[8] E. L. WILSON, L. R. JONES and T. HSUEH, Large displacement analysis of axisymmetric shells, structures and materials research. Report 69-13, University of California, Berkeley, March (1969).
[9] M. KHOJASTEH-BAKHT, Analysis of elastic-plastic shells of revolution under axisymmetric loading by finite element method. Ph.D. Dissertation. Structures and Materials Research Report 67-8, Dept. of Civil Engineering, University of California, Berkeley (1967).
[10] P. SHARIFI and E. D. POPOV, Refined finite element analysis of elastic-plastic thin shells of revolution. Structural and Materials Research Report 69–28, University of California, Berkeley, December (1969)
[11] H. S. LEVINE, H. ARMEN, JR., R. WINTER and A. PIFKO, Nonlinear behavior of shells of revolution under cyclic loading. *National Symposium on Computerized Structural Analysis and Design*, George Washington University, Washington, D.C., 27–29 March (1972); Grumman Research Department Report RE-426J, Bethpage, New York, April (1972).
[12] S. YAGHMAI, Incremental analysis of large deformation in mechanics of solids with applications to axisymmetric shells of revolution. Structures and Materials Research Report 68—17, University of California, Berkeley, December (1968).
[13] D. S. MARGOLIAS, The effect of external loading on the natural frequencies of paraboloidal shells. Ph.D. thesis, University of Southern California, Los Angeles (1970).
[14] H. M. ADELMAN, D. S. CATHERINES and W. C. WALTON, A method for computation of vibration modes and frequencies of orthotropic thin shells of revolution having general meridional curvature. NASA TN D4972, Langley, Virginia, January (1969).
[15] T. HSUEH and E. L. WILSON, Stability analysis of axisymmetric shells. Structures and Materials Research Report 69–22, University of California, Berkeley, September (1969).
[16] P. UNDERWOOD, Transient response of inelastic shells of revolution. *National Symposium on Computerized Structural Analysis and Design*, George Washington University, Washington, D.C., 27–29 March (1972); Lockheed Missiles & Space Company, Inc., Report, LMSC-D244589, Sunnyvale, California, November (1971).
[17] R. E. BALL, A computer program for the geometrically nonlinear static and dynamic analysis of arbitrarily loaded shells of revolution, theory and user's manual. NASA CR 1987, National Aeronautics and Space Administration, Washington, D.C., April (1972).
[18] J. LESTINGI and J. PADOVAN, Numerical analysis of anisotropic rotational shells subjected to nonsymmetric loads. *National Symposium on Computerized Structural Analysis and Design*, George Washington University, Washington, D.C., 27–29 March (1972).
[19] J. C. GERDEEN, F. A. SIMONEN and D. T. HUNTER, Large deflection analysis of elastic-plastic shells using numerical integration. *AIAA J.* 9, (6), 1012–1018 (1971).
[20] R. F. HARTUNG, An assessment of current capability for computer analysis of shell structures. *J. Computers & Structures* 1, 3–32 (1971).
[21] R. F. HARTUNG, An assessment of current capability for computer analysis of shell structures. Air Force Flight Dynamics Laboratory, AFFDL TR 71-54, April (1971).
[22] D. BUSHNELL, Computer analysis of shell structures, *ASME* Paper No. 69-WA/PVP-13, November (1969).
[23] R. E. FULTON, Numerical analysis of shells of revolution. *Proc. Symposium of International Union of Theoretical and Applied Mechanics*, pp. 292–319, Liege, France, August (1970).
[24] J. A. STRICKLIN, Geometrically nonlinear static and dynamic analysis of shells of revolution. *Proc. Symposium of International Union of Theoretical and Applied Mechanics*, pp. 383–411, Liege, France, August (1970).
[25] D. BUSHNELL, Stress, buckling, and vibration of prismatic shells. *AIAA J.* 9, (10), 2004–2013 (1971).
[26] D. BUSHNELL, B. O. ALMROTH and F. BROGAN, Finite-difference energy method for nonlinear shell analysis, *J. Computers & Structures* 1, 361–387 (1971).
[27] D. BUSHNELL, Analysis of ring-stiffened shells of revolution under combined thermal and mechanical loading. *AIAA J.* 9, (3), 401–410 (1971).

[28] D. BUSHNELL, Finite-difference energy models versus finite-element models: two variational approaches in one computer program. Presented at *ONR International Symposium for Numerical and Computer Methods in Structural Mechanics*, Urbana, Illinois, September (1971).

[29] M. S. ANDERSON, R. E. FULTON, W. L. HEARD, JR. and J. E. WALZ, Stress, buckling, and vibration analysis of shells of revolution, computer-oriented analysis of shell structures. Air Force Flight Dynamics Laboratory, AFFDL-TR-71-79, pp. 1173–1246, June (1971).

[30] D. BUSHNELL and S. SMITH, Stress and buckling of nonuniformly heated cylindrical and conical shells. *AIAA J.* **9**, (12), 2314–2321 (1971).

(*Received* 11 *August* 1972)